

Low-Frequency Stochastic Gravitational-Wave Background in *Gaia* DR3 catalogue

V. Akhmetov^{1,2} , L. Filipello^{1,3}, M. Crosta¹, M. G. Lattanzi¹, B. Bucciarelli¹, U. Abbas¹ and F. Santucci¹

¹ INAF - Astronomical Observatory of Torino, via Osservatorio 20, I-10025, Turin, Italy
e-mail: akhmetovvs@gmail.com

² Main Astronomical Observatory, National Academy of Sciences of Ukraine, 27 Akademika Zabolotnoho St, 03143 Kyiv, Ukraine

³ University of Turin, Department of Physics, Via Pietro Giuria 1, Turin, Italy

March 26, 2026

ABSTRACT

Context. In the era of Gravitational Waves observations, searching signals at the very low-frequencies ($< 10^{-7}$ Hz) can bring important constraints on cosmology and the early universe. As the next *Gaia* Data Release (DR4) approaches, high-precision astrometry is emerging as a powerful complement to other methods, such as pulsar timing arrays (PTAs), in the search for gravitational wave backgrounds and discrete sources.

Aims. We investigate the potential to detect low-frequency gravitational waves (GWs) through their imprints on the proper motions of distant quasars observed by the *Gaia* mission. Using astrometric data from *Gaia* DR3, we simulate the effect of GWs on the proper motions of quasars, incorporating their actual sky positions and measurement uncertainties.

Methods. We investigate the two data analysis techniques used for the extraction and characterization of GW signals from quasar proper motions: Vector Spherical Harmonics (VSH) and angular correlation functions, commonly referred to as Hellings–Downs curves (HDC). Using realistic simulated data, we forecast their sensitivity and accuracy to GWs, and evaluate the impact systematic errors might have on them. From these simulations, we derive an upper limit on the amplitude of a stochastic GW background, constrained by the observational timespan, astrometric precision, and the sky distribution of the quasars. Also, we test scalability, as a significantly growing number of quasars with high quality proper motions is expected in the next *Gaia* data release (DR4).

Results. Compared to HDC, VSHs appear more statistically robust, less prone to cherry picking, and with a significantly smaller computational cost, scales as N . The HDC method is more sensitive for detecting gravitational waves, but its complexity scales as N^2 .

Conclusions. We find that, with *Gaia* DR3 proper motions errors, the lower limit for a detectable GW strain is of 10^{-11} , with possible improvements to $\sim 3 \times 10^{-12}$ for the next *Gaia* Data Release 4 (for the same number of quasars). This limit holds for a stochastic spectrum of GW integrated over all frequencies less than half the inverse of the 34 month span of the observations *Gaia* DR3, or about $f_{\text{GW}} \lesssim 5.6$ nHz. We investigated how different data-restriction and weighting schemes influence the final estimate of the gravitational wave strain.

Key words. gravitational waves - astrometry - proper motion - methods: numerical - methods: observational - *Gaia*

1. Introduction

After fully entering the era of Gravitational Wave (GW) astronomy, it has become crucial to leverage expertise from different fields to study these weak-regime gravitational phenomena. Although GWs were not the primary target of the *Gaia* mission, its high-precision astrometry provides a valuable resource for detecting signals in the very-low-frequency regime (Gwinn et al. 1997; Book & Flanagan 2011; *Gaia* Collaboration et al. 2021).

A key aspect of GW detection through astrometry is that, while Pulsar Timing Arrays (PTAs)—the primary experimental method for low-frequency GW detection—are sensitive only to the changes in pulse arrival times caused by GWs along the line of sight (effectively a radial displacement of the pulsar position as projected along the observer’s line of sight), astrometric observations can probe the transverse component of GW perturbations, i.e., the angular motion on the celestial sphere (Hobbs G. et al. 2010; Gwinn et al. 1997). Moreover, because proper motions are secular measurements, the accessible frequency range is bounded by the duration of the mission (upper limit) and the look-back time of the observed quasars (lower limit), which is

strongly dependent on cosmology (Darling 2025). This will further discussed in the following sections.

Assuming that GW-induced angular displacements are the sole contributor to quasar proper motions, it is necessary to employ methods capable of extracting these subtle signals. Two main approaches have been proposed: (i) analysis of angular motions using Vector Spherical Harmonics (VSH) to probe different multipoles Vityazev & Tsvetkov (2009); Mignard & Klioner (2012), and (ii) computation of correlations following a Hellings–Downs curve (HDC) for GW-induced perturbations, examining all possible quasar pairs at varying angular separations Hellings & Downs (1983); Gwinn et al. (1997).

High-precision astrometry complements existing GW detection techniques by providing an independent probe of low-frequency signals. Gravitational waves induce apparent deflections in the positions of distant quasars (QSO), producing correlated proper motions across the sky. The amplitude of the GW strain detectable by astrometry is primarily limited by the astrometric precision, the duration of the observations, and the sky coverage of the quasar sample (Book & Flanagan 2011; *Gaia* Collaboration et al. 2021).

In this work, our aim is to develop a fast and highly parallelized tool for the simulation and analysis of GW-induced astrometric deflections. With future *Gaia* data releases, the number of quasars with proper motions minimally affected by systematics is expected to increase significantly. Consequently, the computational cost will rise for both analysis techniques: Hellings–Downs correlation analysis scales approximately as $O(N^2)$, where N is the number of quasars, whereas higher-order VSH multipoles scale linearly with N . Furthermore, VSH decomposition is found to be statistically robust, less sensitive to uneven quasar sampling, and computationally more efficient compared to HD correlation methods.

In addition, in this weak-regime it is challenging to distinguish systematic errors from genuine physical effects. Therefore, quasars can also serve as a tool to characterize and quantify the magnitude of *Gaia*'s systematics (Lindgren et al. 2021).

In Sect. 2, we first summarize the theoretical tools used to extract and characterize stochastic GW signals from proper motions, followed by a description of the computational techniques adopted for noise reduction and data compression.

In Sect. 3, we evaluate the effects on proper motions due to different types of GW sources on simulated data and examine the possible effects of systematics and anisotropies on the analysis in order to forecast the possible intrinsic limits of astrometric data.

In Sect. 4, we present the data analysis performed on real quasars from *Gaia*-CRF3 (Gaia Collaboration et al. 2022) to estimate current systematic errors and to obtain updated constraints on the low-frequency Gravitational Wave Background.

2. Methods

Astrometric deflections induced by Gravitational Waves can be characterized as angular displacements of distant sources on the celestial sphere. As shown by Book & Flanagan (2011), in the far-away approximation, for an observer at rest (which in the real scenario will be the barycenter of the Solar System), the astrometric displacement of the position u^i of a source in the celestial sphere due to a passing plane GW can be expressed as

$$\delta u^i = \frac{u^i + p^i}{2(1 + \mathbf{u} \cdot \mathbf{p})} h_{jk} u^j u^k - \frac{1}{2} h_{ij} u^j, \quad (1)$$

where vector \mathbf{p} is the propagation direction of the wave, vector \mathbf{u} is the unperturbed direction from the observer to the source at the moment of observation and h_{ij} is the metric perturbation due to the gravitational wave (Pyne et al. 1996). It should be noted that this displacement corresponds to the component with respect to the tetrad of a cosmological static observer, i.e., a hypothetical observer at rest in the cosmological frame. In practice, the Gaia catalog contains processed measurements, where the Gaia RELativistic Model (GREM) reconstructs a single direction per observation (Klioner 2003; Crosta & Vecchiato 2010). Hence, the formula above should be interpreted as the theoretical reference frame, while the actual Gaia measurements include the effects of the data processing and the scanning law.

Right now, QSO are the most promising sources for GW detection with astrometry: they are extremely far extragalactic objects, meaning that their intrinsic proper motion should be way below the angular resolution scale of current optical telescope, therefore the observed proper motions must be caused by the imprint of Gravitational Waves (either resolvable sources or a stochastic background) or other systematic effects. In this setup, the actual observable for studying GW will be an angular

proper motion, i.e. a displacement in sky over a certain time interval Δt . Another key aspect is the frequency domain we can access with astrometric proper motion: these observables are the results of a linear fit from the astrometric solution, therefore they are a secular effect. It follows that, assuming our sensitivity is strong enough for detection and characterization of GWs, any effect on the proper motions from frequencies higher than the inverse of total observation time $1/T$ will be suppressed by the fitting pipeline. On the other hand, the lower limit on accessible frequencies is defined by the QSO lookback time.

It is clear that we are dealing with a different scenario from standard radio astronomy GW search, since these experiments are designed to find periodic signals in a frequency range defined by their Nyquist limit and the total measuring time (roughly 20 years for PTA consortia at the time of writing). Different works have been proposed for the study of GW periodic signals from astrometric time series (Book & Flanagan 2011; Klioner 2018; Darling et al. 2018; Jaraba et al. 2023; Çalışkan et al. 2024; Geyer, R. et al. 2025), but there are still difficult issues to overcome.

Since quasars are extragalactic objects, their lookback time is cosmology dependent, while the time of data acquisition is 34 months for *Gaia* DR3 (Gaia Collaboration et al. (2021) (corresponding to $\sim 11.3 \times 10^{-9}$ Hz) and will reach 10 years for *Gaia* DR5 (corresponding to $\sim 3.2 \times 10^{-9}$ Hz). In this work, we adopt a Λ CDM cosmology with $\Omega_M = 0.315$, $\Omega_\Lambda = 0.685$, and $H_0 = 67 \text{ km s}^{-1} \text{ Mpc}^{-1}$ (Aghanim et al. (2020), from which follows a frequency lower-limit of the order of $\sim 10^{-18}$ Hz).

In this study, we primarily focus on the analysis of methods and their limitations for estimating the amplitude of GWs. We do not investigate the physical properties or nature of the gravitational waves themselves, but rather aim to quantify the statistical prospects for their detection in current astrometric data. To this end, we simulate astrometric deflections of quasar positions for a given GW source direction, amplitude, and frequency, using the formalism described by Geyer, R. et al. (2025). The resulting vector field of apparent positional deflections for the h_+ and h_\times polarizations is illustrated in the figure 1 below.

To extract GW signatures from astrometric data, two main analysis techniques are employed:

(i) Hellings–Downs Correlation (HDC): This approach evaluates the angular correlations of proper motion pairs as a function of their separation, providing a statistical measure of the presence of a stochastic GW background (Hellings & Downs 1983; Gwinn et al. 1997; Darling 2025).

(ii) Vector Spherical Harmonics (VSH): This method decomposes the vector field of proper motions on the celestial sphere into orthogonal multipoles, allowing the separation of GW-induced signals from other astrophysical and systematic effects. (Titov, O. et al. 2011; Klioner 2018; Jaraba et al. 2023; Geyer, R. et al. 2025).

Both methods were implemented within a highly parallelized data-analysis pipeline, combined with GW modeling that accounts for the sky distribution of quasars and the uncertainties of their proper motions from the *Gaia* DR3 catalogue. Appropriate weighting schemes were applied to mitigate the impact of systematic effects in both methods.

The use of simulated astrometric deflections of quasar positions induced by a given GW allows us to assess the impact of the quasar sky distribution, the precision of proper motion measurements in the *Gaia* DR3 catalog, and various data selection criteria on the estimation of the GW amplitude. This analysis is performed using both the Hellings–Downs correlation (HDC) method and the Vector Spherical Harmonics (VSH) approach,

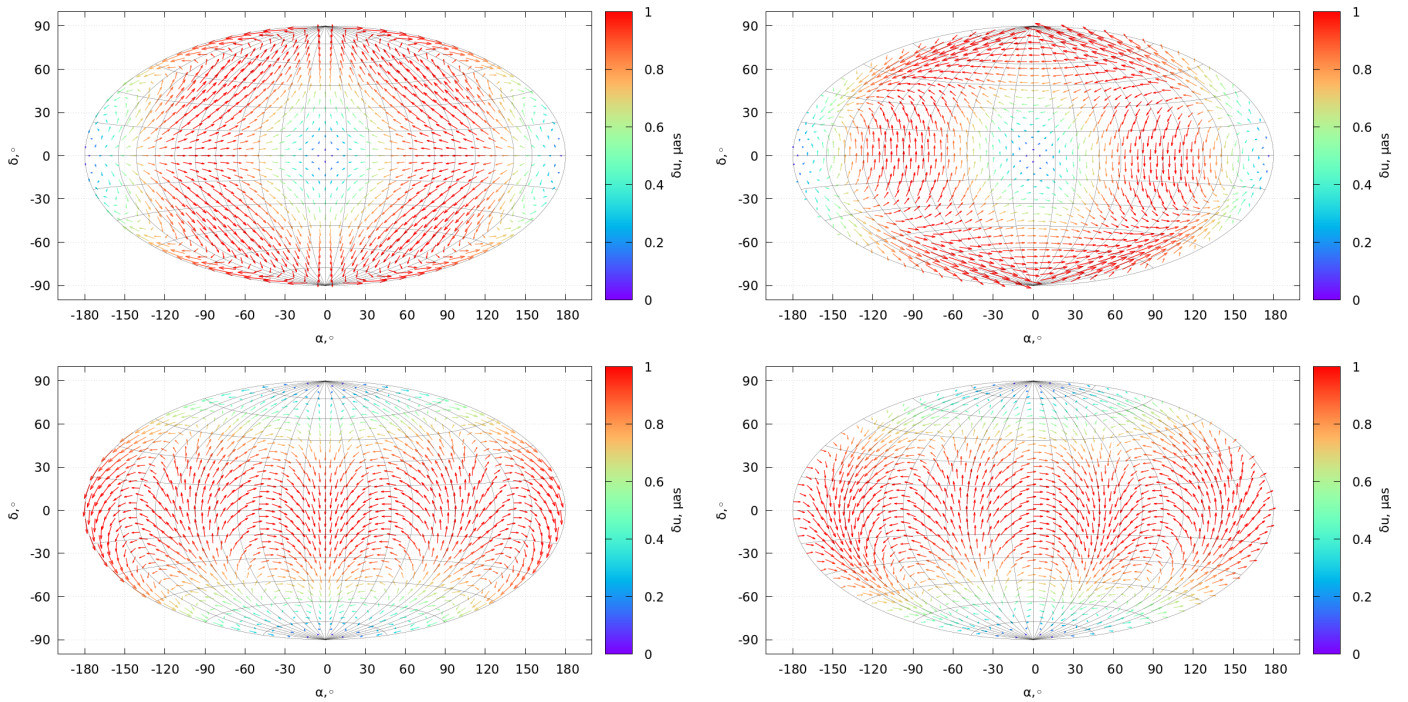


Fig. 1. Simulated apparent positional deflections $\delta\mathbf{u}$ of sources induced by a GW with strain amplitude $h = 10^{-11}$, propagating toward the direction $\alpha = \delta = 0^\circ$ (top panel) and $\alpha = 0^\circ$ and $\delta = 90^\circ$ (bottom panel). The two GW polarizations are shown: "+" (left panel) and "x" (right panel). The vector length and color encode the magnitude of the displacement $|\delta\mathbf{u}|$. The maps use an Aitoff projection in equatorial coordinates.

allowing a comparative evaluation of their sensitivity and accuracy.

2.1. Vector Spherical Harmonics

Since astrometric measurements are defined on the celestial sphere, a natural approach to characterizing vector fields on such manifold is provided by spherical harmonic functions. The application of Vector Spherical Harmonics (VSH (Arfken & Weber 2005)) to the analysis of vector fields defined on the unit sphere originates from the classical expansion of scalar fields in the basis of spherical harmonic functions $Y_{\ell m}(\alpha, \delta)$:

$$\mathbf{Y}_{\ell m}^E = \frac{1}{\sqrt{\ell(\ell+1)}} \nabla Y_{\ell m}(\alpha, \delta), \quad (2)$$

$$\mathbf{Y}_{\ell m}^B = -\frac{1}{\sqrt{\ell(\ell+1)}} \hat{\mathbf{n}} \times \nabla Y_{\ell m}(\alpha, \delta), \quad (3)$$

where the superscripts E and B correspond to the spheroidal (electric-like) and toroidal (magnetic-like) modes, respectively. It follows that any vector field $\mathbf{V}(\alpha, \delta)$ defined on the sphere can be expanded on the VSH basis as

$$\mathbf{V}(\alpha, \delta) = \sum_{\ell=1}^{\infty} \sum_{m=-\ell}^{\ell} (s_{\ell m} \mathbf{Y}_{\ell m}^E(\alpha, \delta) + t_{\ell m} \mathbf{Y}_{\ell m}^B(\alpha, \delta)) \quad (4)$$

with $s_{\ell m}$ and $t_{\ell m}$ are complex expansion coefficients. Within this framework, Vector Spherical Harmonics provide a powerful and flexible tool for studying the statistical and physical properties of quasar proper motions, as demonstrated in several previous works Gwinn et al. (1997); Vityazev & Tsvetkov (2009); Titov, O. et al. (2011); Mignard & Klioner (2012); Gaia Collaboration et al. (2021, 2022).

With VSH, we can already assess the impact of some systematic (and astrophysical) effects on astrometric solutions from the

magnitude of the dipole contributions, i.e. the first order terms in the expansion. The term proportional to \mathbf{Y}_{1m}^E (spheroidal harmonic) is associated to the acceleration toward the Galactic center that the Solar System is experiencing, whereas the term \mathbf{Y}_{1m}^B (toroidal harmonic) is related to a rotation of the reference system (or a rotation of the universe). While the Galactic drift is an astrophysical effect that cannot be eliminated from astrometric measurements (Gaia Collaboration et al. 2021; Brown et al. 2025), an ideal telescope should not exhibit any rotation of the reference frame (assuming that our universe is not rotating related to Mach's principle (Schiff 1964)).

Secular effects to proper motion due to passing GW are expected at quadrupole order $\ell = 2$. Assuming that such effects are caused by a stochastic background, one can relate the magnitude of total quadrupole power (from both E and B modes) to the energy density of the GWB in the universe Ω_{GW} in the following way (Darling et al. 2018):

$$\Omega_{GW} = \frac{6}{5} \frac{P_2}{4\pi^2 H_0^2}, \quad (5)$$

which in our adopted cosmology is equivalent to:

$$\Omega_{GW} = 0.00042 \frac{P_2}{(1\mu\text{as}/\text{yr})^2 h_{70}^{-2}}, \quad (6)$$

where P_2 is the square of the total quadrupole power,

$$P_2 = \sum_{m=-2}^2 (s_{2m}^2 + t_{2m}^2). \quad (7)$$

This equality is valid when the associated Legendre polynomials include the normalization factor $\sqrt{2}$, following the definition of Abramowitz & Stegun (1972), as adopted in Vityazev & Tsvetkov (2009). If a different normalization is used, all harmonics with $m \neq 0$ should be multiplied by an additional factor of

$\sqrt{2}$. Higher multipoles do not have a well-defined astrophysical cause, hence the remaining power at $\ell > 2$ is a useful proxy for assessing the impact of systematic errors in the catalog.

2.2. Pair Correlations

Another possible way of inferring the effects of GWs on astrometric data is the analysis of proper motion correlations for all possible pairs of quasars. For such method, firstly introduced in the context of PTA, one needs to define the angular correlation function (or Hellings-Downs curve Hellings & Downs (1983)) between the GW induced perturbations on two different objects in the sky, which in this scenario comes down to quasars angular motions. Given the fact that proper motions are two dimensional vectors, there is no unique way for defining an Hellings-Downs curve for the its components, but a useful approach has been proposed Moore et al. (2017); Mihaylov et al. (2018); Darling (2025).

To compute the proper motion components required for the astrometric Hellings-Downs analysis, it is necessary to determine the great-circle directions connecting each pair of quasars. In the equatorial system the components of the normal triad [\mathbf{p} \mathbf{q} \mathbf{r}] are given by the matrix:

$$\mathbf{R} = \begin{pmatrix} p_x & q_x & r_x \\ p_y & q_y & r_y \\ p_z & q_z & r_z \end{pmatrix} = \begin{pmatrix} -\sin \alpha & -\sin \delta \cos \alpha & \cos \delta \cos \alpha \\ \cos \alpha & -\sin \delta \sin \alpha & \cos \delta \sin \alpha \\ 0 & \cos \delta & \sin \delta \end{pmatrix} \quad (8)$$

For sphere with radius equal 1 the equatorial components of the proper motion $\hat{\mu}_n$ in direction $\hat{\mathbf{n}}$ may thus be written in matrix form as:

$$\hat{\mathbf{n}} = \begin{pmatrix} n_x \\ n_y \\ n_z \end{pmatrix} = \mathbf{R} \begin{pmatrix} 0 \\ 0 \\ 1 \end{pmatrix}, \quad \hat{\mu} = \begin{pmatrix} \mu_x \\ \mu_y \\ \mu_z \end{pmatrix} = \mathbf{R} \begin{pmatrix} \mu_\alpha^* \\ \mu_\delta \\ 0 \end{pmatrix} \quad (9)$$

In the catalogs, the proper motion in right ascension is typically provided as $\mu_\alpha^* = \mu_\alpha \cos \delta$, where the factor $\cos \delta$ accounts for the convergence of meridians toward the celestial poles, ensuring that the angular displacement along right ascension is expressed in true arc length on the sky.

Two objects with proper motion vectors $\hat{\mu}_n$ and $\hat{\mu}_m$, located in the sky directions $\hat{\mathbf{n}}$ and $\hat{\mathbf{m}}$ are separated by an angular distance θ , given by the dot product:

$$\cos \theta = \hat{\mathbf{n}} \cdot \hat{\mathbf{m}}, \quad (10)$$

where angle θ is the abscissa in the HD curve in Fig. 2.

For each pair of quasar, one needs to find the great circle on the sky connecting them, in order to decompose the proper motions in a component parallel to the great circle ($\hat{\mathbf{e}}_{\parallel,n}$ and $\hat{\mathbf{e}}_{\parallel,m}$) and a perpendicular one $\hat{\mathbf{e}}_{\perp}$:

$$\hat{\mathbf{e}}_{\perp} = \frac{\hat{\mathbf{n}} \times \hat{\mathbf{m}}}{\sqrt{1 - (\hat{\mathbf{n}} \cdot \hat{\mathbf{m}})^2}}, \quad \hat{\mathbf{e}}_{\parallel,n} = \hat{\mathbf{e}}_{\perp} \times \hat{\mathbf{n}}, \quad \hat{\mathbf{e}}_{\parallel,m} = \hat{\mathbf{e}}_{\perp} \times \hat{\mathbf{m}}. \quad (11)$$

As a result, it is possible to define four different astrometric Hellings-Downs correlation curves: one describing the correlation between the parallel components of the proper motions ($C_{\parallel\parallel}$), one for the perpendicular components ($C_{\perp\perp}$), and two cross terms, which are not sensitive to an isotropic stochastic gravitational-wave background ($C_{\perp\perp}$ and $C_{\perp\parallel}$):

$$\begin{aligned} C_{\parallel\parallel}(\theta) &= \langle (\hat{\mu}_n \cdot \hat{\mathbf{e}}_{\parallel,n}) (\hat{\mu}_m \cdot \hat{\mathbf{e}}_{\parallel,m}) \rangle_\theta, \\ C_{\perp\perp}(\theta) &= \langle (\hat{\mu}_n \cdot \hat{\mathbf{e}}_{\perp}) (\hat{\mu}_m \cdot \hat{\mathbf{e}}_{\perp}) \rangle_\theta, \\ C_{\perp\parallel}(\theta) &= \langle (\hat{\mu}_n \cdot \hat{\mathbf{e}}_{\perp}) (\hat{\mu}_m \cdot \hat{\mathbf{e}}_{\parallel,m}) \rangle_\theta, \\ C_{\parallel\perp}(\theta) &= \langle (\hat{\mu}_n \cdot \hat{\mathbf{e}}_{\parallel,n}) (\hat{\mu}_m \cdot \hat{\mathbf{e}}_{\perp}) \rangle_\theta, \end{aligned} \quad (12)$$

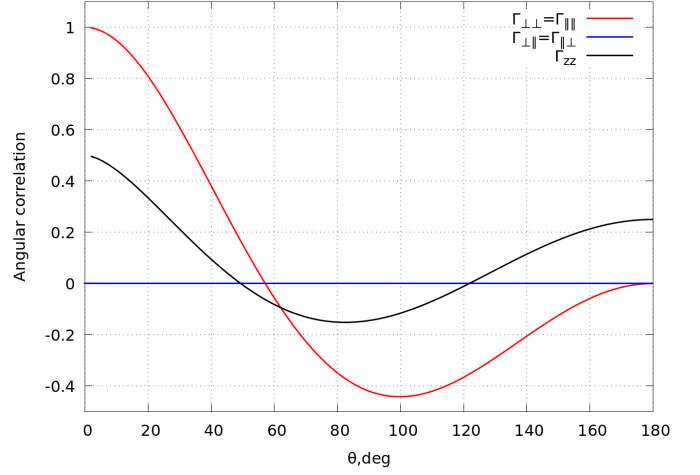


Fig. 2. Hellings-Downs curves for different GW induced displacements. In *red* the parallel-parallel and perpendicular-perpendicular correlation function, in *blue* the cross-terms (trivially zero for an isotropic GWB) and in *black* the radial correlation function as measured by PTA (normalized to $\frac{1}{2}$ due to the non negligible star term for pulsars).

where the angular brackets denote an ensemble average over all source pairs with angular separation θ within a bin of width $\Delta\theta$. While these are the actual observables, we still need to define the expected value from our theoretical model. Starting from the pair correlation of angular displacements in this particular decomposition, and approximating the GWB as an unresolvable superposition of plane waves isotropically distributed on the sky, we get:

$$\langle \delta u_{i,a} \delta u_{j,b}^* \rangle = \frac{1}{24} h_c^2(f) \Gamma_{ab}(\theta), \quad (13)$$

where $a, b \in \{\parallel, \perp\}$, h_c is the characteristic strain of the background and Γ_{ab} is the proper angular correlation functions (the factor $1/24$ comes from the normalization of Γ_{ab} at $\theta = 0$). As shown in (Mihaylov et al. 2018), there is an analytical solution for the angular correlation functions for an isotropic background:

$$\begin{aligned} \Gamma_{\parallel\parallel}(\theta) &= \Gamma_{\perp\perp}(\theta) = 1 - 7 \sin^2\left(\frac{\theta}{2}\right) \\ &\quad - 12 \sin^2\left(\frac{\theta}{2}\right) \tan^2\left(\frac{\theta}{2}\right) \ln\left[\sin\left(\frac{\theta}{2}\right)\right], \\ \Gamma_{zz}(\theta) &= \frac{1}{2}(1 + \beta) + \frac{1}{4} \sin^2\left(\frac{\theta}{2}\right) + 3 \sin^2\left(\frac{\theta}{2}\right) \ln\left[\sin\left(\frac{\theta}{2}\right)\right]. \end{aligned} \quad (14)$$

where $\beta = 1$ for co-located pulsars and is zero otherwise and $\Gamma_{\parallel\perp}(\theta) = \Gamma_{\perp\parallel}(\theta) = 0$. These functions are plotted in Fig. 2, together with the radial correlation function Γ_{zz} as measured by PTA experiments in *black* color.

Additionally, since proper motions correspond to angular deflections measured over a time interval $\Delta t \sim 1/f$, the expected correlation (i.e., the observable quantity) acquires an additional factor of f^2 . This arises because proper motions represent a secular accumulation of angular displacements, so the correlation scales with the square of the frequency of the underlying GW signal.

$$\langle \mu_{i,a} \mu_{j,b} \rangle_\theta = \frac{1}{24} f^2 h_c^2(f) \Gamma_{ab}(\theta), \quad (15)$$

or, alternatively

$$\langle \mu_{i,a} \mu_{j,b} \rangle_\theta = \frac{1}{16\pi^2} H_0^2 \Omega_{GW}^2(f) \Gamma_{ab}(\theta), \quad (16)$$

where again Ω_{GW} is the energy density of Gravitational Waves (Darling et al. 2018).

It is important to note that in the derivation above we assumed that only passing gravitational waves (and white noise) contribute to the QSOs' proper motions. However, as discussed in the previous section, known systematic effects, such as the Galactic acceleration and the rotation of the reference frame, also affect measurements aimed at detecting gravitational waves. Consequently, when performing a pair-correlation analysis using the proper motion from an astrometric catalog, these systematics may introduce spurious correlations.

One way to mitigate this issue is to use vector spherical harmonics (VSH) to estimate the dipole components of the proper motion and to correct the catalog by removing these contributions. After applying these corrections, the Hellings–Downs analysis can be performed on the modified catalog.

3. GW simulation

While in the section 2 we presented a data analysis technique for a GWB, in the case of a perfectly isotropic background the analytical solution of the Hellings–Down correlation function is the same, as we show in Appendix A were approximating the background as a superposition of a large number of independent gravitational waves generated by a population of supermassive black hole binaries (SMBHBs). Therefore, in this scenario, we can effectively use a single source (SS) plane wave as mock signal while still using the same formula presented above. Nevertheless, while the majority of the efforts are towards the detection of a stochastic background, we can still expect some SS signals in this frequency regime (even though discussing the nature of the GW sources is outside the scope of this article).

To investigate the astrometric signature of gravitational waves (GWs) on extragalactic sources, we simulate plane GWs with specified frequencies and propagation directions. As described in Section 2, we investigate the influence of GWs on the proper motions of extragalactic objects by simulating a single plane GW with equal polarizations “+” and “×”, characterized by a strain amplitude $h_+ = h_\times = 10^{-11}$, propagating in the direction $\alpha = 45^\circ$, $\delta = 45^\circ$. The GW frequency is chosen to be inversely proportional to the time baseline of the simulated proper motions, following Geyer, R. et al. (2025).

This framework provides a clear geometric interpretation of the astrometric response: from the observer's perspective, a GW induces a coherent, elliptical motion of all sources across the celestial sphere. The eccentricity of these ellipses is identical for all sources and is determined solely by the strain parameters of the wave, whereas their sizes and orientations also depend on the angular separation between the source direction and the GW propagation direction. A key outcome of this formulation is that the astrometric signature of a GW is, in some respects, analogous to that of astrometric binary systems. The essential distinction, however, is that a GW produces a globally correlated signal, simultaneously affecting all sources on the sky.

In this limiting case, the GW signal manifests itself as a synchronized circular motion of all sources on the sky, with an amplitude that depends only on the angle between the source direction and the direction of GW propagation. The maximum amplitude of the deviation on the sky occurs for a source located perpendicular to the GW propagation direction ($\theta = 90^\circ$) while sources lying nearly along the propagation direction ($\theta = 0^\circ$ or $\theta = 180^\circ$) are hardly deflected, as illustrated in Figure 1.

One of the key objectives of this work, which we demonstrate here, is to investigate the effect of non-uniform quasar

distributions and inhomogeneous proper motion uncertainties, together with their correlations, on the detectability of gravitational waves.

3.1. Noise-free case

In Figure 3 (*left panel*), we show the Hellings–Downs (HD) curves obtained from simulated proper motions of 30 000 uniformly distributed sources located at the centers of HEALPix pixels with $n_{\text{side}}=50$ (Górski et al. 2005). As seen in Figure 3 (*top of the left panel*), in the noise-free case, the correlation components $C_{\perp\perp}$ and $C_{\parallel\parallel}$ are equal and match the theoretical HD curves, while the cross terms, which are not sensitive to GWs ($C_{\parallel\perp}$ and $C_{\perp\parallel}$), remain zero for all angular separations θ .

We performed a similar simulation of GW without adding noise, but using the actual positions of 1.5 million quasars from the *Gaia*-CRF3 catalog. As shown in Figure 3 (*top of the right panel*), the correlation components $C_{\perp\perp}$ and $C_{\parallel\parallel}$ do not coincide for angular separations $\theta > 40^\circ$ and deviate slightly from the theoretically expected HD curve.

It is also noteworthy that the cross terms ($C_{\parallel\perp}$ and $C_{\perp\parallel}$), which are expected to be zero in the idealized uniform case, become non-zero starting from $\theta > 20^\circ$. They vary within certain ranges of θ and reach deviations up to 25% of the amplitude of $C_{\perp\perp}$ and $C_{\parallel\parallel}$.

This demonstrates that a non-uniform sky distribution of sources significantly affects the detectability of gravitational waves and the accuracy of parameter estimation using the Hellings–Downs correlation method.

Figure 3 (*bottom row*) presents the dependence of the power of the vector spherical harmonics (VSH), P_l , on the harmonic degree l , obtained from the simulated data. These plots illustrate how the total power P is distributed across harmonic degrees l , highlighting the quadrupole ($l = 2$) signal induced by a plane GW. As shown in the *bottom left panel* of Fig. 3, the powers of the toroidal and spheroidal harmonics coincide for all harmonic degrees, as expected for a GW induced astrometric signal.

GWs do not contribute to the dipole ($l = 1$) harmonics, which is consistent with the quadrupole nature of GW. The dominant contribution appears at the quadrupole order ($l = 2$), where the measured power agrees with the theoretically expected value of $P_2^T = P_2^S \approx 3.7 \mu\text{as}^2 \text{yr}^{-2}$. The power of higher-order harmonics decreases by approximately an order of magnitude with increasing l , indicating that the astrometric response is strongly dominated by the lowest non-vanishing multipole.

The physical origin of the dominance of the $l = 2$ harmonics lies in the quadrupolar nature of GWs. A plane gravitational wave induces a coherent, large-scale quadrupolar distortion of the apparent positions of sources on the celestial sphere, which is naturally captured by the $l = 2$ VSH components. The values of P_l thus directly reflect the relative amplitudes of the astrometric signal induced by a GW at different VSH degrees (Klioner 2018).

As shown in the *bottom right panel* of Fig. 3, the non-uniform sky distribution of quasars in the *Gaia*-CRF3 catalogue has a negligible impact on the estimated power of the vector spherical harmonics. This indicates that the VSH method is largely insensitive to inhomogeneities in the sky coverage of the sources. In contrast, the Hellings–Downs correlation (HDC) method exhibits a strong dependence on the degree of uniformity of the source distribution.

This difference arises from the fact that the VSH formalism represents the global astrometric signal as an orthogonal expansion over the full sky, where the power at a given harmonic de-

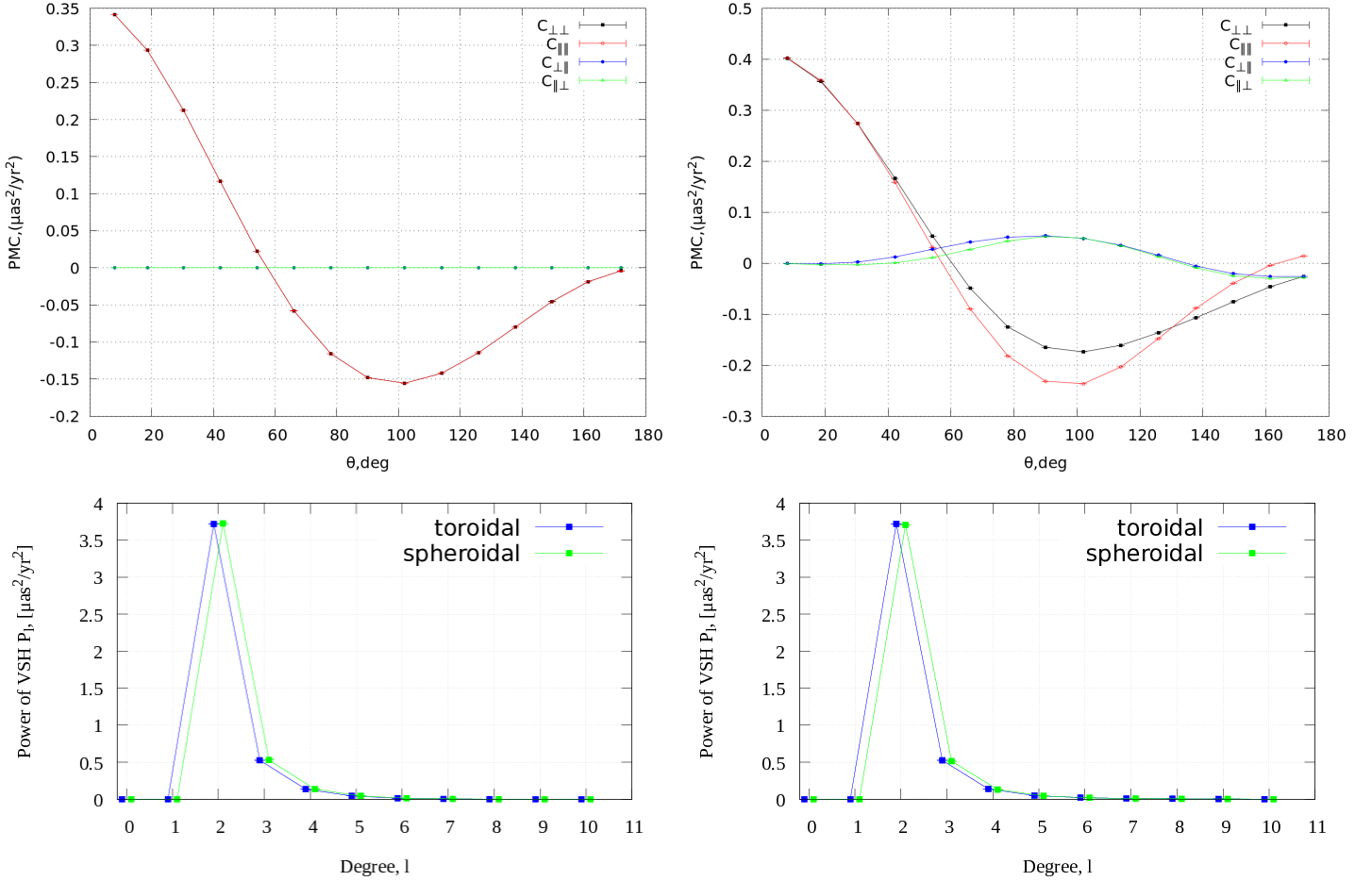


Fig. 3. The *top row* shows the Hellings–Downs curves for all four proper motion correlation (PMC) components, calculated from noise-free simulated data for a uniform sky distribution of sources (*top left panels*) and for the actual distribution of 1.5 million quasars from the *Gaia*-CRF3 catalog (*top right panels*). The *bottom row* presents the power spectra of the vector spherical harmonics (VSH) coefficients, P_l , for the same simulated datasets. For clarity, the toroidal (*blue*) and spheroidal (*green*) harmonic points are horizontally offset by $\Delta l = 0.1$. The simulations assume a plane gravitational wave with equal “+” and “ \times ” polarizations, characterized by a strain amplitude $h_c = 10^{-11}$, propagating in the direction $\alpha = 45^\circ$, $\delta = 45^\circ$.

gree is obtained by integrating contributions from all directions. As a result, local variations in source density tend to average out and primarily affect the statistical uncertainty rather than biasing the recovered harmonic power.

In contrast, the HDC method relies on pairwise correlations between sources at given angular separations. For a non-uniform sky distribution, certain angular bins become over- or under-sampled, leading to biased correlation estimates and increased leakage between correlation components. Consequently, the HDC approach is significantly more sensitive to sky inhomogeneities than the VSH-based analysis.

3.2. Noise case

To investigate the impact of observational uncertainties on the detection of GWs, we perform simulations including Gaussian noise in the quasar proper motions. The noise is modeled using the covariance matrices of the *Gaia*-CRF3 proper motions, taking into account both the standard errors in proper motion uncertainties and their correlation:

$$\mathbf{Cov} = \begin{pmatrix} \sigma_{\mu_\alpha}^2 & \rho\sigma_{\mu_\alpha}\sigma_{\mu_\delta} & 0 \\ \rho\sigma_{\mu_\alpha}\sigma_{\mu_\delta} & \sigma_{\mu_\delta}^2 & 0 \\ 0 & 0 & 0 \end{pmatrix} \quad (17)$$

where σ_{μ_α} and σ_{μ_δ} are the standard errors of the proper motions in right ascension and declination, respectively, ρ is the correlation coefficient between the proper motion components in right ascension and declination.

This noise is scaled according to the proper motion uncertainties of the 1.5 million quasars in the *Gaia*-CRF3 catalog (selected using criteria described in Sec. 4.1) using lower-triangular Cholesky matrix $\mathbf{L}\mathbf{L}^T = \mathbf{Cov}$ and defined as:

$$\mathbf{L} = \begin{pmatrix} \sigma_{\mu_\alpha} & 0 & 0 \\ \rho\sigma_{\mu_\alpha}\sigma_{\mu_\delta} & \sigma_{\mu_\delta} & 0 \\ 0 & 0 & \sqrt{1 - \rho^2}\sigma_{\mu_\alpha}\sigma_{\mu_\delta} \end{pmatrix} \quad (18)$$

Then, the contribution of Gaussian noise in the modeling of proper motions can be represented as additional components $\delta\mu_\alpha$ and $\delta\mu_\delta$, which are determined using the formula:

$$\begin{pmatrix} \delta\mu_\alpha \\ \delta\mu_\delta \\ 0 \end{pmatrix} = \mathbf{L} \begin{pmatrix} g_1 \\ g_2 \\ 0 \end{pmatrix} \quad (19)$$

where g_1 and g_2 are independent Gaussian random variables with $\sigma = 1$. This procedure ensures correlated Gaussian perturbations consistent with the observed uncertainties and correlation of quasars proper motions in *Gaia*-CRF3.

Our main assumption is that the simulated quasar proper motions contain only the distortions induced by the modeled GW, combined with Gaussian noise. Although this represents an idealized scenario, it allows us to isolate the GW signal and to systematically evaluate the performance of the analysis methods considered in this work.

An accurate determination of the Hellings–Downs correlation curve requires a correct weighting of the measured proper motions. This weighting must account for both the uncertainties of the proper motion components and their correlation coefficients. Under these conditions, the components of the covariance matrix in the cartesian equatorial coordinate system can be expressed as follows: $\hat{C}ov = \mathbf{R}Cov\mathbf{R}^T$, where \mathbf{R}^T denotes the transpose of the normal triad matrix defined in (8). To correctly weight the proper motions when computing the correlation curve, it is necessary to obtain the scalar projection of the covariance matrix $\hat{C}ov$ along the direction parallel to the great circle $\hat{e}_{||}$ defined by two objects with sky directions $\hat{\mathbf{n}}$ and $\hat{\mathbf{m}}$, as well as along the perpendicular direction \hat{e}_{\perp} :

$$\begin{aligned}\sigma_{||,n}^2 &= \hat{e}_{||,n}^T \cdot \hat{C}ov_n \cdot \hat{e}_{||,n}, & \sigma_{\perp,n}^2 &= \hat{e}_{\perp}^T \cdot \hat{C}ov_n \cdot \hat{e}_{\perp}, \\ \sigma_{||,m}^2 &= \hat{e}_{||,m}^T \cdot \hat{C}ov_m \cdot \hat{e}_{||,m}, & \sigma_{\perp,m}^2 &= \hat{e}_{\perp}^T \cdot \hat{C}ov_m \cdot \hat{e}_{\perp}.\end{aligned}\quad (20)$$

where \hat{e}^T denotes the transpose of the unit vector corresponding to the great-circle direction for a given object, defined using Eqs. 11. The total variance of the proper motion uncertainties projected onto these directions for a pair of objects is then given by the following expressions:

$$\begin{aligned}W_{|||} &= (\hat{\boldsymbol{\mu}}_n \cdot \hat{e}_{||,n})^2 \sigma_{||,m}^2 + (\hat{\boldsymbol{\mu}}_m \cdot \hat{e}_{||,n})^2 \sigma_{||,n}^2 + \sigma_{||,n}^2 \sigma_{||,m}^2, \\ W_{\perp\perp} &= (\hat{\boldsymbol{\mu}}_n \cdot \hat{e}_{\perp})^2 \sigma_{\perp,m}^2 + (\hat{\boldsymbol{\mu}}_m \cdot \hat{e}_{\perp})^2 \sigma_{\perp,n}^2 + \sigma_{\perp,n}^2 \sigma_{\perp,m}^2, \\ W_{\perp||} &= (\hat{\boldsymbol{\mu}}_n \cdot \hat{e}_{\perp})^2 \sigma_{||,m}^2 + (\hat{\boldsymbol{\mu}}_m \cdot \hat{e}_{||,m})^2 \sigma_{\perp,n}^2 + \sigma_{\perp,n}^2 \sigma_{||,m}^2, \\ W_{||\perp} &= (\hat{\boldsymbol{\mu}}_n \cdot \hat{e}_{||,n})^2 \sigma_{\perp,m}^2 + (\hat{\boldsymbol{\mu}}_m \cdot \hat{e}_{\perp})^2 \sigma_{||,n}^2 + \sigma_{||,n}^2 \sigma_{\perp,m}^2.\end{aligned}\quad (21)$$

Finally, this variances are used to weight the proper motion correlations $C_{ab}(\theta)$ for all possible combinations:

$$\begin{aligned}C_{|||}(\theta) &= \langle (\hat{\boldsymbol{\mu}}_n \cdot \hat{e}_{||,n})(\hat{\boldsymbol{\mu}}_m \cdot \hat{e}_{||,n})/W_{|||} \rangle_{\theta} / \langle W_{|||} \rangle_{\theta}, \\ C_{\perp\perp}(\theta) &= \langle (\hat{\boldsymbol{\mu}}_n \cdot \hat{e}_{\perp})(\hat{\boldsymbol{\mu}}_m \cdot \hat{e}_{\perp})/W_{\perp\perp} \rangle_{\theta} / \langle W_{\perp\perp} \rangle_{\theta}, \\ C_{\perp||}(\theta) &= \langle (\hat{\boldsymbol{\mu}}_n \cdot \hat{e}_{\perp})(\hat{\boldsymbol{\mu}}_m \cdot \hat{e}_{||,m})/W_{\perp||} \rangle_{\theta} / \langle W_{\perp||} \rangle_{\theta}, \\ C_{||\perp}(\theta) &= \langle (\hat{\boldsymbol{\mu}}_n \cdot \hat{e}_{||,n})(\hat{\boldsymbol{\mu}}_m \cdot \hat{e}_{\perp})/W_{||\perp} \rangle_{\theta} / \langle W_{||\perp} \rangle_{\theta}\end{aligned}\quad (22)$$

If the weighting coefficient is assumed to be equal to unity (i.e., all proper motions are assigned equal weights), this expression reduces to 12.

In realistic astrometric catalogs such as *Gaia*-CRF3, the uncertainties of the proper motion components are heteroscedastic, and the errors in μ_{α}^* and μ_{δ} are generally correlated. Because the observation equations have different uncertainties and include correlated errors, the statistically optimal solution is obtained using the generalised least-squares (GLS) method.

Stacking the equations for all sources, the GLS estimator of the VSH coefficient vector \mathbf{x} is given by:

$$\mathbf{x} = (\mathbf{A}^T Cov^{-1} \mathbf{A})^{-1} \mathbf{A}^T Cov^{-1} \boldsymbol{\mu}, \quad (23)$$

where \mathbf{A} is the design matrix $2N \times m$ contains the values of the m VSH basis functions evaluated at the positions of all N sources, Cov^{-1} is the inverse of the full covariance matrix of the proper motions (see Eq. 17), and $\boldsymbol{\mu}$ is the $2N$ -dimensional proper motion vector. The number of equations is twice the number of sources

because, for each source, two equations are included: one for μ_{α}^* and one for μ_{δ} .

Using the Cholesky decomposition of each source covariance (see Eq. 18), and multiplying the observation equations by \mathbf{L}^{-1} yields the transformed system of equations:

$$\tilde{\boldsymbol{\mu}} = \tilde{\mathbf{A}}\mathbf{x} + \tilde{\boldsymbol{\varepsilon}}, \quad (24)$$

with

$$\tilde{\boldsymbol{\mu}} = \mathbf{L}^{-1}\boldsymbol{\mu}, \quad \tilde{\mathbf{A}} = \mathbf{L}^{-1}\mathbf{A}. \quad (25)$$

where $\tilde{\boldsymbol{\varepsilon}}$ is the ‘‘weighted and de-correlated noise’’ after accounting for the correlations and the different uncertainties between μ_{α}^* and μ_{δ} . This transformation effectively standardizes the scale of the errors and de-correlates them. The problem then reduces to an ordinary least-squares (OLS) solution applied to these transformed equations.

Appendix B.1 presents a comparison of the HDC and VSH methods for estimating the GW amplitude using the same simulated dataset, highlighting the differences between analyses performed with and without weighting schemes.

Figure 4 (*top left panel*) presents the Hellings–Downs (HD) correlation curves derived from simulations of GW that include noise, using the actual *Gaia*-CRF3 quasar positions together with their proper motion uncertainties and correlations. The inclusion of noise further amplifies the deviations of the $C_{\perp\perp}$ and $C_{|||}$ components from the theoretical HD curve and introduces additional scatter. This clearly highlights the combined impact of uneven sky coverage and non-uniform proper motion uncertainties on the detectability of gravitational waves and on the accuracy of parameter estimation using the HD correlation method. The cross terms ($C_{\perp||}$ and $C_{||\perp}$) depart from zero over the entire range of angular separations θ , demonstrating that uncertainties in quasar proper motions contribute significantly to the observed correlations, in addition to the effects of their non-uniform distribution on the celestial sphere.

Despite the substantial scatter of the correlation components shown in Fig. 4 (*top left panel*), we performed a fit of the correlation components using the functional form given by Eq. 14. This yields a value of $0.4238 \pm 0.1281 \mu\text{as}^2\text{yr}^{-2}$ (fig. 4 *top right panel*), which is very close to the model expectation of $0.3533 \mu\text{as}^2\text{yr}^{-2}$. The 95% confidence interval shown in this figure *in green* corresponds to the uncertainty of the fitted amplitude parameter of the Hellings–Downs correlation function.

The *bottom left panel* of Fig. 4 shows the VSH power as a function of the harmonic degree ℓ , calculated from simulated proper motions for the actual quasar sky distribution, with *Gaia*-CRF3 error-dependent noise added. As can be seen, the power of the $\ell = 2$ harmonics significantly exceeds the expected values that were introduced into the proper motions through the simulated gravitational wave. Higher-order harmonics also appear, resulting from the superposition of several factors: significant noise in the proper motions and its dependence on the source positions. It can be concluded that the non-uniform sky distribution of sources, combined with substantial proper motion uncertainties and the presence of correlations, leads to a spurious increase in the inferred GW amplitude by a factor of 3–5 when using the VSH method.

However, if the random component of the proper motions is reduced by a factor of three, i.e., using $0.3\sigma_{\mu_{\alpha}^*}$ and $0.3\sigma_{\mu_{\delta}}$ in Eq. 18, as expected in the next data release *Gaia* DR4, the VSH method allows a successful detection of gravitational waves with a strain amplitude $h_c = 10^{-11}$, as shown in the *bottom right panel* of Fig. 4.

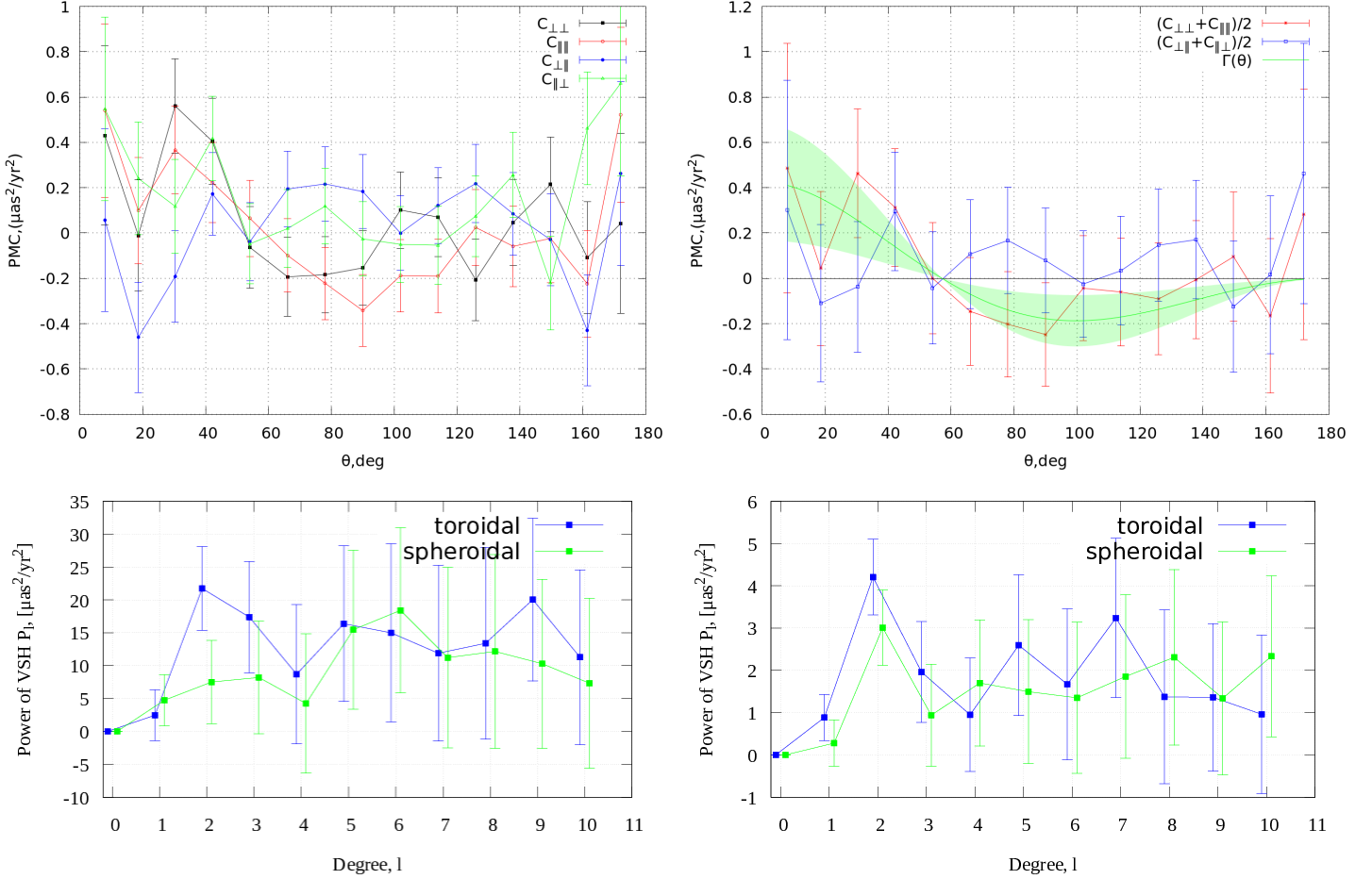


Fig. 4. The *top row* shows the Hellings–Downs curves for all four proper motion correlation (PMC) components, calculated from simulated proper motions for the actual quasar sky distribution, with *Gaia*-CRF3 error-dependent noise added (*top left panel*). The *top right panel* presents the averaged correlation components $C_{\perp\perp}$ and $C_{\parallel\parallel}$ (red), together with the cross terms ($C_{\perp\parallel}$ and $C_{\parallel\perp}$) (blue). Also shown are the fitted Hellings–Downs function $\Gamma(\theta)$ and its corresponding 95% confidence interval (green), derived from these correlation curves. The *bottom row* shows the power spectra of the vector spherical harmonics (VSH) coefficients P_l for the same simulated dataset (*bottom left panel*), and for a simulation in which the quasar proper motion uncertainties are reduced by a factor of three, as expected for future *Gaia* DR4 (*bottom right panel*). For clarity, the toroidal (blue) and spheroidal (green) harmonic points are horizontally offset by 0.1 in l . The simulations assume a plane GW with equal “+” and “x” polarizations, characterized by a strain amplitude $h_c = 10^{-11}$, propagating in the direction $\alpha = 45^\circ$, $\delta = 45^\circ$.

As seen in the *bottom right panel* of Fig. 4, the power of the second-order harmonics for the toroidal (B-mode) and spheroidal (E-mode) components are similar and consistent with the expected values within their respective uncertainties. Almost all higher-order harmonic powers do not exceed their measurement errors, and their amplitudes are roughly an order of magnitude smaller than in the *bottom left panel*, confirming the three-fold reduction in proper motion uncertainties.

Thus, we conclude that the VSH method is more statistically robust, less sensitive to uneven objects sampling and more sensitive to noise in gravitational wave detection but is computationally faster. The computational complexity of the VSH method scales linearly with the number of sources N . In contrast, the HDC method is more sensitive for detecting gravitational waves, but its complexity scales as N^2 and more prone to cherry picking. Therefore, applying the HDC method to AGIS residuals or to catalogs containing tens of millions of sources requires appropriate algorithmic modifications and the use of parallel computations on GPUs.

This result suggests that, given the statistical precision of the proper motions for the 1.5 million quasars in the *Gaia*-CRF3 catalog, the Hellings–Downs correlation method could detect grav-

itational waves with a strain amplitude of $h_c \gtrsim 10^{-11}$ at a significance level of 3σ .

However, this conclusion holds only under idealized assumptions, namely: (i) the absence of systematic errors in the *Gaia* catalogue, and (ii) a regime in which a portion of the GW-induced elliptical motion can be approximated by a linear trend corresponding to a constant proper motion. This occurs when the GW period is approximately twice the observation time, $P_{\text{GW}} \approx 2 T_{\text{obs}}$ (Gwinn et al. 1997). In the opposite limits, the signal is either largely absorbed by the AGIS astrometric solution ($P_{\text{GW}} \ll 2 T_{\text{obs}}$) or varies too slowly to produce a measurable proper motion signature ($P_{\text{GW}} \gg 2 T_{\text{obs}}$).

In reality, the presence of systematic errors in the *Gaia* catalog, as well as a mismatch between the observational time span and the gravitational wave period, can significantly suppress the GW signature in quasar proper motions, as demonstrated by (Geyer, R. et al. 2025). Consequently, under realistic conditions, the upper limit on the detectable GW strain amplitude using the Hellings–Downs correlation method is expected to be higher by a factor of approximately 2–3 using data of *Gaia*-CRF3 quasars.

4. Results

4.1. *Gaia*-CRF3 catalogue analysis

We apply both the Hellings–Downs correlation (HDC) method and the vector spherical harmonics (VSH) approach to the *Gaia*-CRF3 catalogue (Gaia Collaboration et al. 2022). In practice, the true proper motions of quasars are expected to be essentially zero. However, due to the limited astrometric precision of the *Gaia* measurements, the observed proper motions are non-zero and dominated by measurement noise. The systematic contribution to the proper motions caused by the acceleration of the solar system barycentre and by gravitational waves (and also, possibly, the presence of systematic errors) is at the level of a few $\mu\text{s yr}^{-1}$, which is several orders of magnitude smaller than the typical proper motion uncertainties.

For each quasar, an effective signal-to-noise ratio can be defined as

$$(S/N)^2 = \frac{1}{1 - \rho^2} \left[\frac{\mu_\alpha^2}{\sigma_{\mu_\alpha}^2} + \frac{\mu_\delta^2}{\sigma_{\mu_\delta}^2} - 2\rho \frac{\mu_\alpha \mu_\delta}{\sigma_{\mu_\alpha} \sigma_{\mu_\delta}} \right], \quad (26)$$

A moderate threshold of $S/N < 3$ is applied to reject the sources with high proper motions while retaining a sufficiently large number of quasars. In addition, we apply a quality cut of $\text{RUWE} < 1.2$ (Renormalised Unit Weight Error), which is a reliable goodness of fit statistic selecting sources with well behaved astrometric solutions. This combined selection balances the trade-off between reducing measurement noise and maintaining a sample size large enough to reliably detect the correlated signal induced by gravitational waves. As a result, we obtain a final sample comprising positions, proper motions, their uncertainties, and correlations for 1 505 427 quasars. Statistical properties of the selected quasar sample from the *Gaia*-CRF3 catalogue are presented in Table 1.

As a first step in the analysis of the proper motions of the selected quasar sample, we applied the vector spherical harmonics (VSH) formalism to estimate and remove large-scale systematic effects, represented by the lowest-order harmonics. These terms account for the residual rotation of the celestial reference frame and for the apparent dipole pattern induced by the acceleration of the Solar System barycentre.

Figure 5 (*top left panel*) presents the power of the VSH coefficients as a function of harmonic degree, while the *top right panel* shows the corresponding mean power of each toroidal or spheroidal harmonic using formula $\bar{P}_l = P_l / (2l + 1)$. The mean power derived from our sample is in good agreement with the results presented by (Gaia Collaboration et al. 2022), confirming the overall consistency of the large-scale astrometric systematics in the *Gaia*-CRF3 catalogue. It is also worth noting that the powers of higher-order harmonics derived from the actual proper motions of *Gaia*-CRF3 quasars are roughly an order of magnitude larger than the corresponding powers obtained from simulated proper motions (see the *bottom left panel* of Fig. 4). This indicates that the *Gaia*-CRF3 catalogue likely contains significant systematic errors, which manifest not only in the higher-order harmonics but also substantially affect GW detection. This supports our conclusion from the previous section that systematic and proper motion uncertainties have a major impact on the GW detection level, effectively raising the upper limit on detectable GW amplitudes by times. The powers $\sqrt{P_2^s}$ and $\sqrt{P_2^t}$ derived from the *Gaia*-CRF3 data, as reported in Table 2, indicate an apparent GW strain amplitude $h_c \sim 4.5 \times 10^{-11}$. As shown by the simulations in the previous section, the combination of

non-uniform source distribution, significant proper motion uncertainties, and correlations leads to a spurious amplification of the GW amplitude by a factor of 3–5 when calculated using the VSH analysis.

Figure 5 (*bottom left panel*) presents the correlation components $C_{\perp\perp}$ and $C_{\parallel\parallel}$, together with the cross terms ($C_{\parallel\perp}$ and $C_{\perp\parallel}$). Also the (*bottom right panel*) shows the averaged correlation components and the best-fitting Hellings–Downs correlation function $\Gamma(\theta)$ and its corresponding 95% confidence interval (*green*), derived after applying a dipole-mode correction based on the proper motions of quasars from the *Gaia*-CRF3 catalogue. The amplitude obtained from the HDC analysis is $h_c \sim 9.0 \times 10^{-11}$, indicating a significant impact of higher-order harmonics (systematics) on the shape and amplitude of the resulting correlation curve.

The apparent amplitude of the GW strain, $h_c \sim 4.5$ or 9×10^{-11} , is unnaturally high and is therefore more likely to be associated with significant systematic and random errors in the *Gaia*-CRF3 catalogue than with a true GW signal.

Table 2 lists the estimated VSH coefficients of first and second degree (dipole and quadrupole components). The application of vector spherical harmonics is described in detail, for example, in Vityazev & Tsvetkov (2009). Following this formalism, we decompose the VSH coefficients into their real and imaginary parts, which results in a set of harmonics denoted as $s_{\ell,m,p}$ and $t_{\ell,m,p}$. Here, the index ℓ specifies the degree of the harmonic, while m denotes its order. The index p takes two possible values, $p = 0$ and $p = 1$, corresponding to the imaginary and real parts of the harmonic, respectively. Although the overall amplitudes of these harmonics are broadly consistent with previous studies, we find statistically significant differences with respect to the values reported by Darling (2025). These discrepancies are most likely driven by a combination of factors: (i) differences in the adopted quasar selection criteria and sky coverage, and (ii) differences in the treatment of the full astrometric covariance information, in particular the neglect of correlations between the proper motion components in the *Gaia* catalogue (Storey-Fisher et al. 2024). The latter effect is expected to have a non-negligible impact on the estimated amplitudes of VSH harmonics.

4.2. Truncated *Gaia*-CRF3 catalogue analysis

In this subsection, we construct a quasar subsample following the selection criteria presented in Darling (2025), i.e., we select all quasars with proper motion amplitudes less than $100 \mu\text{s yr}^{-1}$. This results in a catalogue containing 70,268 quasars. Table 3 lists the VSH coefficients of the first and second degree (dipole and quadrupole components) derived from this subsample. As shown in Table 4, the average uncertainty of quasar proper motions is approximately $250 \mu\text{s yr}^{-1}$.

As seen in Fig. 6, selecting quasars with small proper motion amplitudes preferentially reduces the large-scale, low-degree VSH modes ($\ell = 1-6$), which dominate the coherent systematic signal, while leaving higher-degree harmonics ($\ell \geq 7$), dominated by small-scale noise, largely unaffected. This effect is purely selection-driven and results from two factors: (i) the pronounced selection-induced non-uniformity in the sky distribution of quasars, primarily dictated by the *Gaia* scanning law, and (ii) the projection of correlated proper motion noise onto low-frequency (low-degree) components. Such a selection suppresses or neglects global systematic patterns in quasar proper motions.

Since the GW signal is encoded predominantly in the lowest-degree vector spherical harmonics, in particular the quadrupolar ($\ell = 2$) modes, selecting on small proper motion amplitudes sys-

Table 1. Statistical properties of the selected sample of 1 505 427 quasars from the *Gaia*-CRF3 catalogue.

Parameter	Mean	SD	Minimum	Maximum	Median	Skewness	Kurtosis
μ_α^* ($\mu\text{as yr}^{-1}$)	-0.68	793	-8 521	8 728	3.26×10^{-2}	-0.008	6.609
μ_δ ($\mu\text{as yr}^{-1}$)	-1.37	736	-8 566	9 297	-1.23×10^{-2}	-0.010	6.839
$\sigma_{\mu_\alpha^*}$ ($\mu\text{as yr}^{-1}$)	653	476	9.72	3 365	516	1.583	2.872
σ_{μ_δ} ($\mu\text{as yr}^{-1}$)	606	441	12.98	3 387	478	1.670	3.396

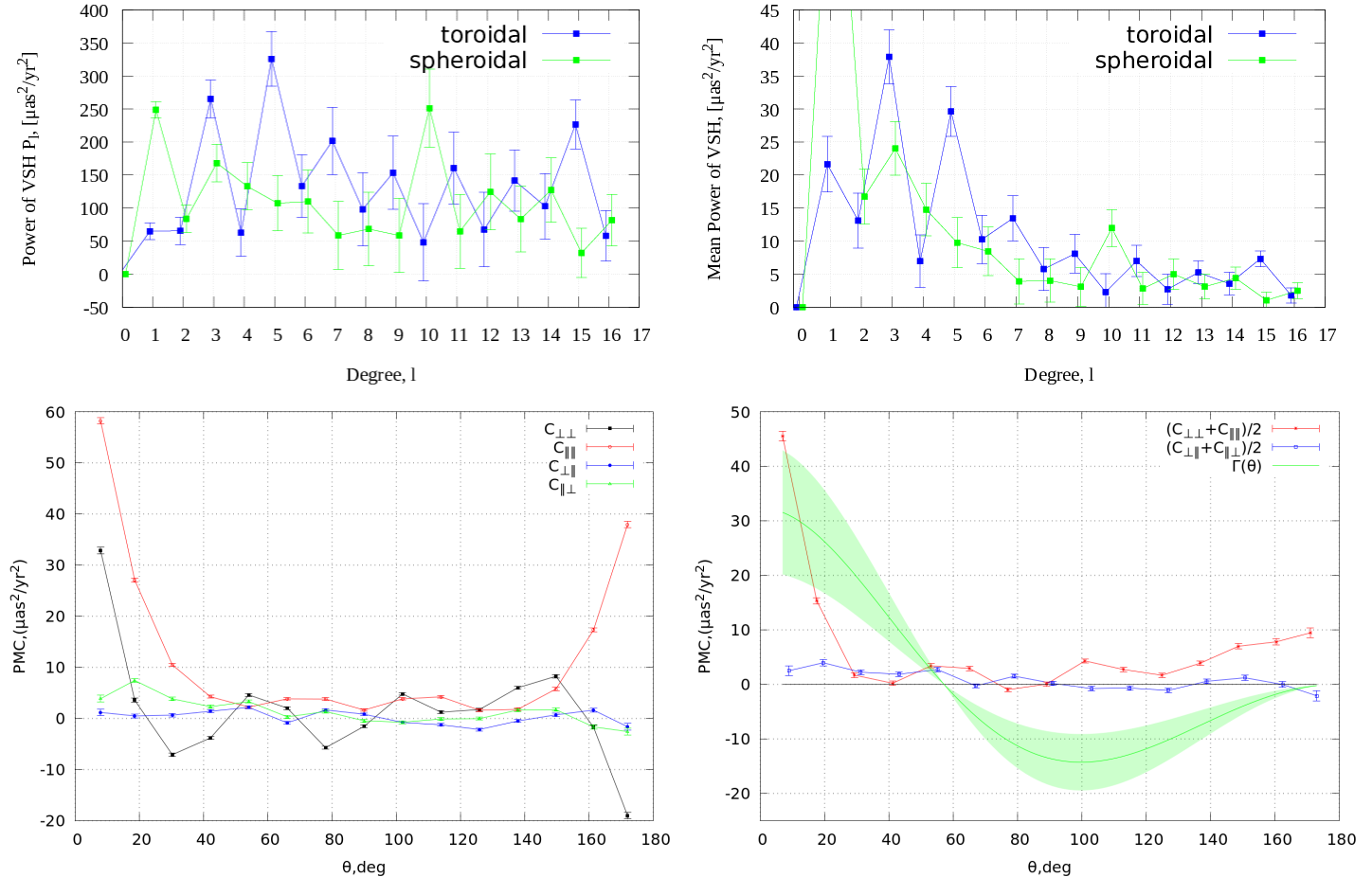


Fig. 5. The *top row* shows the power spectra of the vector spherical harmonic coefficients (*left panel*) and the mean toroidal and spheroidal powers (*right panel*) characterizing systematics in the proper motions of ~ 1.5 million quasars from the *Gaia*-CRF3 catalogue. For clarity, the toroidal (*blue*) and spheroidal (*green*) harmonic coefficients are horizontally offset by $\Delta\ell = 0.1$. The *bottom row* displays the correlation components $C_{\perp\perp}$ and $C_{\parallel\parallel}$ together with the cross terms $C_{\perp\parallel}$ and $C_{\parallel\perp}$ (*left panel*). Also the *right panel* shows the averaged correlation components and the best-fitting Hellings–Downs correlation function $\Gamma(\theta)$ with its corresponding 95% confidence interval (*green*), obtained after applying a dipole-mode correction based on the proper motions of ~ 1.5 million *Gaia*-CRF3 quasars.

tematically reduces the very components that carry the GW information. Consequently, both VSH- and HDC-based analyses applied to such a truncated sample yield biased, systematically underestimated values of the GW strain amplitude. Therefore, selection based on proper motion cannot be regarded as statistically unbiased and may lead to misestimation of the GW signal.

As shown in Table 4, the selected subsample shows a dispersion of proper motions that is significantly smaller than the mean formal uncertainties, together with a negative kurtosis indicative of a truncated distribution. This implies that the applied selection strongly suppresses the tails of the proper motion distribution, resulting in an artificially reduced variance. A kurtosis value close to -1 further indicates that the distribution approaches a nearly uniform form within the selected interval rather than a Gaussian one. Such truncation can bias the estimation of GW-induced cor-

relations and lead to a systematic underestimation of the recovered GW amplitude, as shown in the analysis of simulated data in Appendix B.2 and B.3. In Appendix B.2 and B.3, we examine how various selection criteria applied to simulated quasar proper motions influence both the statistical significance of the detection and the inferred amplitude of the simulated GW signal, as estimated using the VSH and HDC methods.

5. Conclusions

In this work, we investigate the impact of gravitational waves (GWs) on the proper motions of quasars in the *Gaia*-CRF3 catalogue. To this end, we simulate a plane gravitational wave and quantify its contribution to distortions in quasar proper motions. Gaussian noise, proportional to the proper motion uncertainties

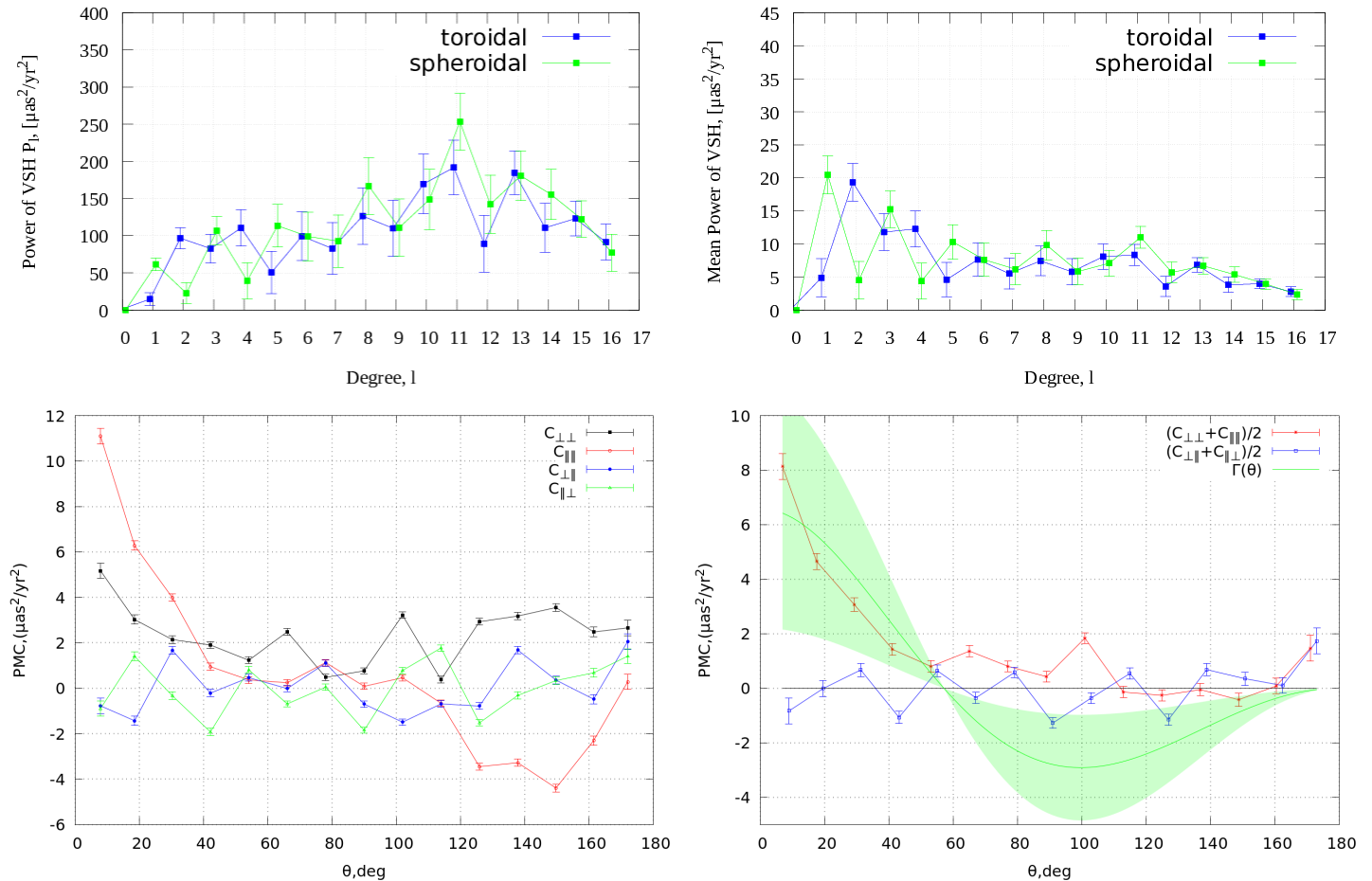


Fig. 6. The same that is on Fig. 5 but for the selected 70 268 *Gaia*-CRF3 quasars with proper motion amplitude less than $100 \mu\text{as yr}^{-1}$.

Table 2. Vector spherical harmonic (VSH) coefficients of degree $l = 1$ (dipole) and $l = 2$ (quadrupole) derived from the 1.5 million *Gaia*-CRF3 quasar sample, in units of $\mu\text{as yr}^{-1}$.

B Modes (Toroidal)			E Modes (Spheroidal)		
Parameter	Value	Unc.	Parameter	Value	Unc.
Dipole ($l = 1$)					
$t_{1,0,1}$	-1.219	2.256	$s_{1,0,1}$	-10.418	1.883
$t_{1,1,0}$	4.202	1.733	$s_{1,1,0}$	-11.083	1.665
$t_{1,1,1}$	6.763	2.128	$s_{1,1,1}$	4.161	2.518
$\sqrt{P_1^t}$	8.05	3.18	$\sqrt{P_1^s}$	15.77	3.42
Quadrupole ($l = 2$)					
$t_{2,0,1}$	1.195	2.247	$s_{2,0,1}$	-0.548	1.916
$t_{2,1,0}$	-1.583	2.350	$s_{2,1,0}$	7.073	2.097
$t_{2,1,1}$	-2.402	1.653	$s_{2,1,1}$	-4.049	1.761
$t_{2,2,0}$	-7.091	2.167	$s_{2,2,0}$	-3.120	2.599
$t_{2,2,1}$	-2.338	1.674	$s_{2,2,1}$	-2.671	1.691
$\sqrt{P_2^t}$	8.09	3.08	$\sqrt{P_2^s}$	9.14	3.39

and their correlations, is also included. We have developed a method to accurately compute the correlation components, accounting for both measurement uncertainties and correlations between proper motions. Our results demonstrate that the non-uniform distribution of quasars significantly affects the proper motion correlation components in the HDC method, whereas the impact on the VSH method is considerably smaller.

Table 3. Vector spherical harmonic (VSH) coefficients of degree $l = 1$ (dipole) and $l = 2$ (quadrupole) derived from the 70,268 quasar *Gaia*-CRF3 sample, in units of $\mu\text{as yr}^{-1}$.

B Modes (Toroidal)			E Modes (Spheroidal)		
Parameter	Value	Unc.	Parameter	Value	Unc.
Dipole ($l = 1$)					
$t_{1,0,1}$	-2.12	1.90	$s_{1,0,1}$	-6.94	1.57
$t_{1,1,0}$	-0.93	1.40	$s_{1,1,0}$	1.36	1.33
$t_{1,1,1}$	-3.05	1.74	$s_{1,1,1}$	3.36	2.10
$\sqrt{P_1^t}$	3.83	2.93	$\sqrt{P_1^s}$	7.83	2.94
Quadrupole ($l = 2$)					
$t_{2,0,1}$	2.00	1.83	$s_{2,0,1}$	-3.55	1.54
$t_{2,1,0}$	0.24	1.97	$s_{2,1,0}$	1.49	1.74
$t_{2,1,1}$	-5.55	1.35	$s_{2,1,1}$	-2.08	1.44
$t_{2,2,0}$	-3.69	1.80	$s_{2,2,0}$	1.04	2.18
$t_{2,2,1}$	-6.94	1.38	$s_{2,2,1}$	-1.53	1.41
$\sqrt{P_2^t}$	9.83	3.77	$\sqrt{P_2^s}$	4.75	3.77

The HDC method provides higher raw statistical sensitivity due to its quadratic scaling with the number of source pairs, but is more susceptible to non-uniform sky coverage and systematic errors. In contrast, the VSH approach enables a robust, mode-resolved characterization of the correlated signal, offering improved control over systematics and a clearer physical interpretation, albeit with reduced statistical sensitivity. In practice, the

Table 4. Statistical properties of 70,268 selected *Gaia*-CRF3 quasars with proper motion amplitudes below $100 \mu\text{as yr}^{-1}$.

Name	Mean	SD	Minimum	Maximum	Median	Skewness	Kurtosis
μ_α^* ($\mu\text{as yr}^{-1}$)	0.0818	48.85	-99.92	100.00	0.234	-0.006	-0.95
μ_δ ($\mu\text{as yr}^{-1}$)	-0.263	48.98	-99.89	99.94	-0.347	0.002	-0.96
σ_{μ_α} ($\mu\text{as yr}^{-1}$)	261.82	213.79	9.72	2882.98	202.21	2.78	13.20
σ_{μ_δ} ($\mu\text{as yr}^{-1}$)	248.90	198.03	12.98	2695.03	195.63	2.96	15.59

two methods are complementary and yield mutually consistent constraints on the presence of GWs.

Analysis of simulated proper motions from the *Gaia*-CRF3 catalogue, including measurement uncertainties and correlations, indicates a theoretical upper limit for GW detection of $h_c \sim 10^{-11}$ using the HDC method. However, systematic errors in the catalogue proper motions, combined with a non-optimal ratio of the GW period to the *Gaia* observation duration, lead to significant absorption of GW-induced distortions into the AGIS residuals, effectively increasing the practical upper limit of the detectable GW amplitude by several times.

Correct weighting of quasar proper motions, taking into account the full covariance matrix, significantly improves the reliability of GW amplitude estimation in both HDC and VSH analyses. The uncertainties of the inferred Gamma function and the VSH power spectrum are reduced by nearly an order of magnitude compared to unweighted analyses. Moreover, the quadrupolar harmonic ($\ell = 2$) dominates the VSH power spectrum as expected, indicating that weighted analyses effectively preserve the large-scale geometric signature of the GW signal while minimizing the impact of spatially inhomogeneous measurement errors.

The precision of quasar proper motions in *Gaia* improves with mission duration because proper motions are estimated as linear trends in position over time. For a uniformly sampled astrometric time series with total baseline T , the proper motion uncertainty scales approximately as $\sigma_\mu \propto T^{-3/2}$, reflecting both the longer observational baseline and the increasing number of measurements. This improvement directly enhances sensitivity to GWs. In the HDC analysis, the statistical uncertainty of the correlation components scales as $\sigma_C \propto \sigma_\mu^2 / \sqrt{N_{\text{pair}}}$, whereas in the VSH approach the uncertainty of each harmonic coefficient scales as $\sigma_{s,\ell} \propto \sigma_\mu / \sqrt{2N}$, where N is the number of quasars. Consequently, the expected $T^{-3/2}$ improvement in proper motion precision from *Gaia* DR3 to DR5 translates into roughly an order-of-magnitude increase in GW sensitivity for both HDC- and VSH-based analyses.

6. Data availability

The used catalogue data are available in a standardized format for readers via the CDS (<https://cds.u-strasbg.fr>). The software code used in this paper can be made available on personal request by e-mail: akhmetovvs@gmail.com.

7. Acknowledgements

This work has made use of data from the European Space Agency (ESA) mission *Gaia* (<https://www.cosmos.esa.int/gaia>), processed by the *Gaia* Data Processing and Analysis Consortium (DPAC, <https://www.cosmos.esa.int/web/gaia/dpac/consortium>). Funding for the DPAC has been provided by national institutions, in particular the institutions participating in the *Gaia* Multilateral Agreement. L.F., M.C., U.A. acknowledge support from the PRIN 2022 grant

20227MYL2X “General Relativistic Astrometry and Pulsar Experiment (GRAPE) financed by the European Union - Next Generation EU, Mission 4 Component 1 CUP C53D23000890006.

References

- Abramowitz, M. & Stegun, I. A. 1972, Handbook of Mathematical Functions
Aghanim, N. et al. 2020, A&A, 641, A6, [Erratum: Astron.Astrophys. 652, C4 (2021)]
Arfken, G. B. & Weber, H. J. 2005, Mathematical methods for physicists 6th ed. Book, L. G. & Flanagan, E. E. 2011, Phys. Rev. D, 83, 024024
Brown, A. G. A., Bastian, U., & Klioner, S. 2025, A&A, 695, A272
Çalışkan, M., Chen, Y., Dai, L., et al. 2024, J. Cosmology Astropart. Phys., 2024, 030
Crosta, M. & Vecchiato, A. 2010, A&A, 509, A37
Darling, J. 2025, ApJ, 982, L46
Darling, J., Truebenbach, A. E., & Paine, J. 2018, ApJ, 861, 113
Gaia Collaboration, Klioner, S. A., Lindegren, L., et al. 2022, A&A, 667, A148
Gaia Collaboration, Klioner, S. A., Mignard, F., et al. 2021, A&A, 649, A9
Gaia Collaboration, Brown, A. G. A. et al. 2021, Astron. Astrophys., 649, A1, [Erratum: Astron.Astrophys. 650, C3 (2021)]
Geyer, R., Klioner, S. A., Lindegren, L., & Lammers, U. 2025, A&A, 695, A172
Górski, K. M., Hivon, E., Banday, A. J., et al. 2005, ApJ, 622, 759
Gwinn, C. R., Eubanks, T. M., Pyne, T., Birkinshaw, M., & Matsakis, D. N. 1997, The Astrophysical Journal, 485, 87
Hellings, R. W. & Downs, G. S. 1983, ApJ, 265, L39
Hobbs G., Archibald A., Arzoumanian Z., et al. 2010, Classical and Quantum Gravity, 27, 084013
Jaraba, S., García-Bellido, J., Kuroyanagi, S., Ferraiuolo, S., & Braglia, M. 2023, Monthly Notices of the Royal Astronomical Society, 524, 3609
Klioner, S. A. 2003, AJ, 125, 1580
Klioner, S. A. 2018, Classical and Quantum Gravity, 35, 045005
Lindegren, L., Klioner, S. A., Hernández, J., et al. 2021, A&A, 649, A2
Mignard, F. & Klioner, S. 2012, Astron & Astrophys., 547, A59
Mihaylov, D. P., Moore, C. J., Gair, J. R., Lasenby, A., & Gilmore, G. 2018, Phys. Rev. D, 97, 124058
Moore, C. J., Mihaylov, D. P., Lasenby, A., & Gilmore, G. 2017, Phys. Rev. Lett., 119, 261102
Pyne, T., Gwinn, C. R., Birkinshaw, M., Eubanks, T. M., & Matsakis, D. N. 1996, ApJ, 465, 566
Schiff, L. I. 1964, Reviews of Modern Physics, 36, 510
Storey-Fisher, K., Hogg, D. W., Rix, H.-W., et al. 2024, Astrophys. J., 964, 69
Titov, O., Lambert, S. B., & Gontier, A.-M. 2011, A&A, 529, A91
Valtolina, Serena, Shaifullah, Golam, Samajdar, Anuradha, & Sesana, Alberto. 2024, A&A, 683, A201
Vityazev, V. V. & Tsvetkov, A. S. 2009, Astronomy Letters, 35, 100

Appendix A: Simulation of a Stochastic Gravitational-Wave Background

To assess the astrometric response of a quasar sample to a stochastic gravitational wave background (SGWB), we performed dedicated simulations in which the background was modeled as a superposition of a large number of independent gravitational waves generated by a population of supermassive black hole binaries (SMBHBs), as these are the most promising GWB candidates. This population was created from a simulated catalog compatible with PTA data Valtolina, Serena et al. (2024).

Roughly 120 000 binaries were uniformly distributed on the sky, and from each source a contribution to the background was calculated from the physical parameters of the catalog (i.e. chirp mass, frequency, physical distance and inclination) plus a random phase. The total GW signal was then constructed as the linear superposition of the plane waves produced by all emitters. As a result, we obtained a time-dependent, spatially varying GW-induced deformation field corresponding to an effectively isotropic source distribution.

The induced apparent proper motions of quasars were computed from the resulting metric perturbations. The expected proper motion field obtained from this superposition is shown in Fig. A.1 (*lower right panel*). The *upper panel* of Fig. A.1 presents the proper motion correlation components derived using the Hellings–Downs correlation method. As seen from figure A.1, even for a uniform distribution of GW sources across the sky, the correlations do not follow the theoretical slope. The cross-correlation terms ($C_{\parallel\perp}$ and $C_{\perp\parallel}$) do not vanish at all angular separations due to the anisotropic spatial distribution of QSOs in optical catalogs. In principle, for future detectors, such effect might become an insurmountable obstacle for the detection of GWB anisotropies with astrometry: implementation of more quantitative and robust analysis will be developed in future works.

Moreover, also the parallel and perpendicular correlation components ($C_{\parallel\parallel}$ and $C_{\perp\perp}$) deviates from expected Hellings–Down curve with two different slopes (even though they should have identical behaviour). However, taking the average values mitigates these effects caused by QSOs spatial distribution and cosmic variance: as shown in the *upper right panel* in figure A.1, the fit can reconstruct the correct characteristic strain from the $(C_{\parallel\parallel} + C_{\perp\perp})/2$ correlation term, showing that the large-scale geometric signature of the background remains dominated by the quadrupolar correlation structure characteristic of gravitational waves.

The *lower left panel* of Fig. A.1 shows the power spectrum of the toroidal (*blue points*) and spheroidal (green points) vector spherical harmonics. The distribution of power across modes confirms that the resulting signal retains the characteristic low-degree structure expected from GW-induced distortions.

We emphasize the fact that such catalog was designed for PTA periodic signal detection, therefore some binaries will have an orbiting frequency higher than current *Gaia* DR3 frequency upper limit. However, here we are not interested in a fully realistic scenario, but rather we want to estimate the geometric structure of astrometric distortion and the effects that the anisotropic distribution of QSOs might have on GWB induced observables. This approach provides a practical upper-limit estimate of the level of correlated proper motion patterns that could be present in real astrometric data.

Appendix B: Checking of selection criteria and weighting scheme

In this appendix, we investigate how different selection criteria and weighting schemes applied to quasar proper motions affect the recovered GW signal when using both the HDC and VSH methods.

To this end, we simulate a plane GW from a single source with the parameters specified in Sect. 3. Gaussian noise is then added to the simulated proper motions. The noise is modeled using the covariance matrices of the *Gaia*-CRF3 proper motions, taking into account both the standard uncertainties of the proper motion components and their correlations (Sect. 3.2).

To obtain a more reliable estimate of the amplitude of the simulated GW signal and to approximate the expected improvement in the forthcoming *Gaia* DR4 release, the noise level is reduced by a factor of three, i.e., $\sigma_{\mu_\alpha} \rightarrow 0.3\sigma_{\mu_\alpha}$ and $\sigma_{\mu_\delta} \rightarrow 0.3\sigma_{\mu_\delta}$. The statistical properties of the simulated proper motions and their corresponding uncertainties for 1.5 million quasars are listed in Table B.1. As seen from the table, the standard deviations of the simulated proper motions are close to the mean uncertainties reported in the *Gaia*-CRF3 catalog, which have been reduced by a factor of three. Moreover, the skewness and kurtosis of the simulated proper motion distribution closely the corresponding values derived from the real data, as listed in Table 1. This indicates that the simulated dataset realistically reproduces the statistical characteristics of the observed quasar sample, making it suitable for testing analysis methods such as HDC and VSH.

Appendix B.1: Comparison of weighted and unweighted approaches

In this subsection we investigate how the application of statistical weights affects the estimation of the GW amplitude derived from simulated quasar proper motions. In particular, we compare two approaches: (i) an unweighted analysis, in which all quasars contribute equally to the statistics in both the HDC and VSH methods, and (ii) a weighted analysis, in which each measurement is weighted according to its formal uncertainty.

The weighted scheme accounts for the heterogeneous astrometric precision of sources in the *Gaia*-CRF3 catalogue. In practice, quasars with smaller proper-motion uncertainties receive larger statistical weights, while objects with larger uncertainties contribute less to the final estimator.

In the HDC framework, the proposed weighting scheme allows different weights to be assigned to the proper-motion components projected along the directions parallel and perpendicular to the great circle connecting each pair of sources. As a result, the same quasar may have different effective weights depending on the specific source pair and on the projected component of the proper motion considered in the correlation analysis (formulas 20, 21 and 22).

To quantify the impact of weighting, we apply both approaches to the same set of simulated proper motions described in Sect. 3. In the *top panel* of Figure B.1, the Hellings–Downs (HD) correlation curves are shown, derived from simulated gravitational waves (GWs) with added noise, using the actual *Gaia*-CRF3 quasar positions together with their proper motion uncertainties and correlations. When unweighted statistics of quasar proper motions are used, neither the HDC nor the VSH method provides a reliable recovery of the model GW amplitude. The uncertainty of the inferred Γ function, derived from the proper motion correlation components, exceeds its estimated value,

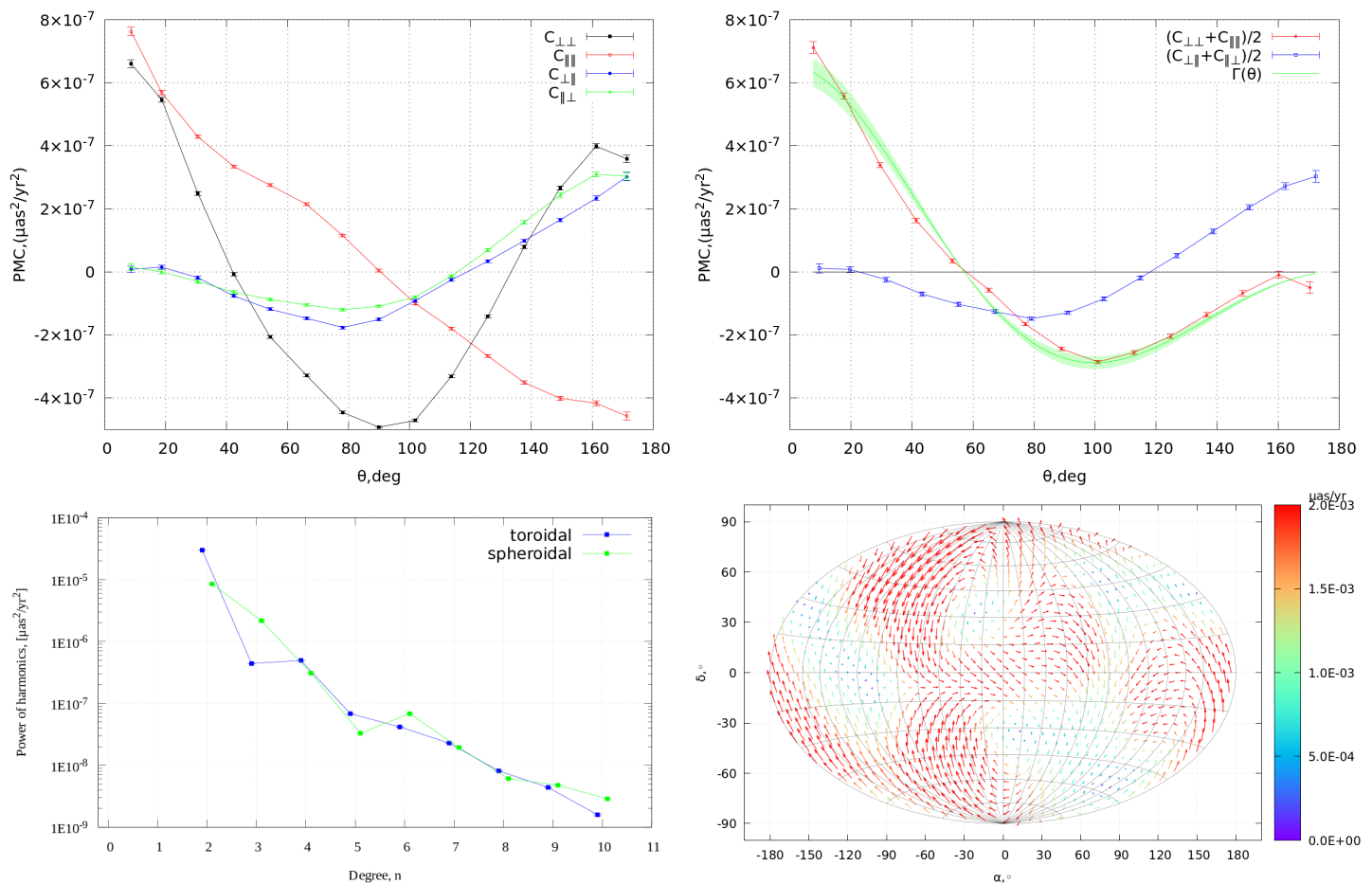


Fig. A.1. The *top left* row presents the proper motion correlation components derived using the Hellings–Downs correlation (HDC) method for all four proper motion correlation (PMC) components, computed from the simulated SGWB. The *top right* panel shows the averaged correlation components $C_{\perp\perp}$ and $C_{\parallel\parallel}$ (red), together with the cross terms $C_{\perp\parallel}$ and $C_{\parallel\perp}$ (blue). Also shown are the best-fitting Hellings–Downs function $\Gamma(\theta)$ and its corresponding 95% confidence interval (green), derived from these correlation curves. The *bottom left* panel displays the power spectrum of the toroidal (blue points) and spheroidal (green points) vector spherical harmonics obtained from the simulated SGWB. The expected proper motion field resulting from the simulated SGWB is shown in the *bottom right* panel. The simulations were performed without including observational uncertainties in quasar proper motions in order to estimate the intrinsic amplitude of the geometric distortions induced by the SGWB.

which is nearly an order of magnitude smaller than the injected model amplitude (*top right* panel). From the *bottom* panel of Figure B.1, it is also evident that the recovered powers of all harmonics do not exceed their corresponding uncertainties and remain in the range of $5\text{--}15 \mu\text{as}^2 \text{yr}^{-2}$. Moreover, high-order harmonics dominate the power spectrum, indicating a highly non-uniform, high-frequency distribution of proper-motion errors across the sky, which is associated with the *Gaia* scanning law.

The *top panels* of Figure B.2 show the Hellings–Downs (HDC) correlation components, while the *bottom panels* display the power spectrum of the VSH harmonics. It is evident that using the correct weighting scheme, which fully accounts for the covariance matrix of quasar proper motions, allows a reliable recovery of the model GW amplitude. The uncertainty of the inferred $\Gamma(\theta)$ function is less than 10% of its value and the value is consistent with the injected model amplitude. Similarly, among the recovered VSH powers, the quadrupolar component P_2 clearly dominates over the higher-order harmonics and closely matches the expected theoretical value. The uncertainties in both the correlation components and the VSH powers are nearly an order of magnitude smaller than in the unweighted case. This demonstrates that the correct weighting of quasar

proper motions is essential for accurate estimation of GW amplitudes and for maximizing the sensitivity of both the HDC and VSH methods. In addition, correct weighting mitigates spurious contributions arising from non-uniform sky coverage, reduces the impact of high-frequency noise, and ensures that large-scale systematic patterns in the proper-motion field are properly captured.

Appendix B.2: Moderate proper-motion selection

We first apply a moderate selection criterion by retaining only quasars with total proper motion amplitudes smaller than $100 \mu\text{as} \text{yr}^{-1}$. This results in a sample of 464 279 quasars. The statistical properties of this subsample are summarized in Table B.2.

As shown in Fig. B.3, the recovered correlation components are approximately a factor of two smaller than the expected theoretical values. Since the GW strain amplitude scales with the square root of the correlation signal, this implies an underestimation of the recovered GW amplitude by a factor of $\sqrt{2}$.

A similar effect is observed in the lower panel of Fig. B.3, where the VSH power spectrum is shown. The quadrupolar ($\ell = 2$) power is reduced by approximately a factor of two relative

Table B.1. Statistical properties of the simulated proper motions for 1 505 427 quasars, with the noise level reduced by a factor of three relative to the *Gaia*-CRF3 catalogue.

Name	Mean	SD	Minimum	Maximum	Median	Skewness	Kurtosis
μ_α^* ($\mu\text{as yr}^{-1}$)	0.0633	250	-3301	3607	0.0460	-0.00524	7.46
μ_δ ($\mu\text{as yr}^{-1}$)	0.104	233	-3044	3136	0.135	-0.0230	7.97
$\sigma_{\mu_\alpha^*}$ ($\mu\text{as yr}^{-1}$)	201	148	2.92	1010	158	1.583	2.872
σ_{μ_δ} ($\mu\text{as yr}^{-1}$)	187	138	3.89	1016	147	1.671	3.396

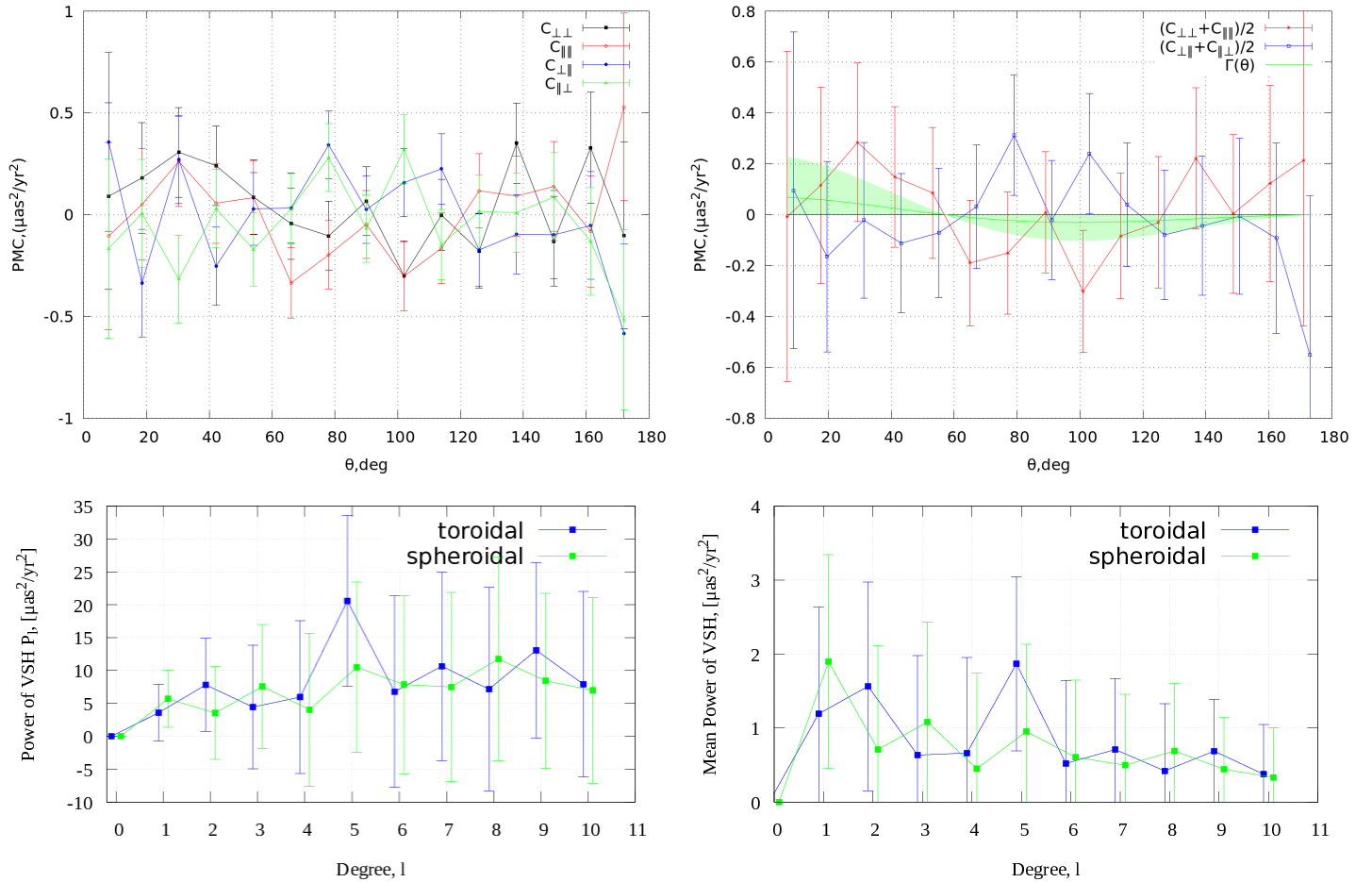


Fig. B.1. Unweighted analysis. The *top row* shows Hellings–Downs curves for all four PMC components from simulated proper motions with the *Gaia*-CRF3 error model (*top left*), and the averaged components $C_{\perp\perp}$, $C_{\parallel\parallel}$ (red) with cross terms $C_{\perp\parallel}$, $C_{\parallel\perp}$ (blue) and the fitted Hellings–Downs function $\Gamma(\theta)$ with 95 % confidence interval (green, *top right*). The *bottom row* shows the power spectra of VSH coefficients (*left*) and mean powers (*right*) for toroidal (blue) and spheroidal (green); coefficients are offset by $\Delta\ell = 0.1$ for clarity. Simulations assume a plane GW with equal “+” and “ \times ” polarizations, $h_c = 10^{-11}$, propagating toward $\alpha = 45^\circ$, $\delta = 45^\circ$, with the random proper motion component reduced by a factor of three ($0.3\sigma_{\mu_\alpha^*}$, $0.3\sigma_{\mu_\delta}$), for a sample of 1 505 427 quasars.

to the injected model. This demonstrates that even a moderate selection based on proper motion amplitude leads to a systematic suppression of the GW signal.

Appendix B.3: Strict proper-motion selection

We next apply a more stringent selection criterion, analogous to that adopted by Darling (2025). Since the simulated noise level in our model is reduced by a factor of three relative to *Gaia*-CRF3, we impose a proportional constraint on the proper motion amplitudes in order to preserve the ratio $|\mu|/\sigma_\mu$.

Specifically, we select quasars with total proper motion amplitudes not exceeding $33 \mu\text{as yr}^{-1}$. This yields a sample of 84 607 quasars, comparable in size to the sample analyzed in

Sect.4.2 and to that used by Darling (2025). This allows us to assess, using simulated data, how such a strict selection affects the recovered GW signal.

The statistical properties of this subsample are listed in Table B.3. The upper panel of Fig.B.4 shows the recovered correlation components and the corresponding Hellings–Downs curve. The amplitude of the recovered correlation function is approximately an order of magnitude smaller than the injected model prediction, implying an underestimation of the GW strain amplitude by a factor of $\sqrt{10}$ (i.e., more than three).

In contrast, the lower panel of Fig.B.4 presents the VSH power spectrum. The quadrupolar ($\ell = 2$) harmonic remains suppressed by approximately a factor of two relative to the expected

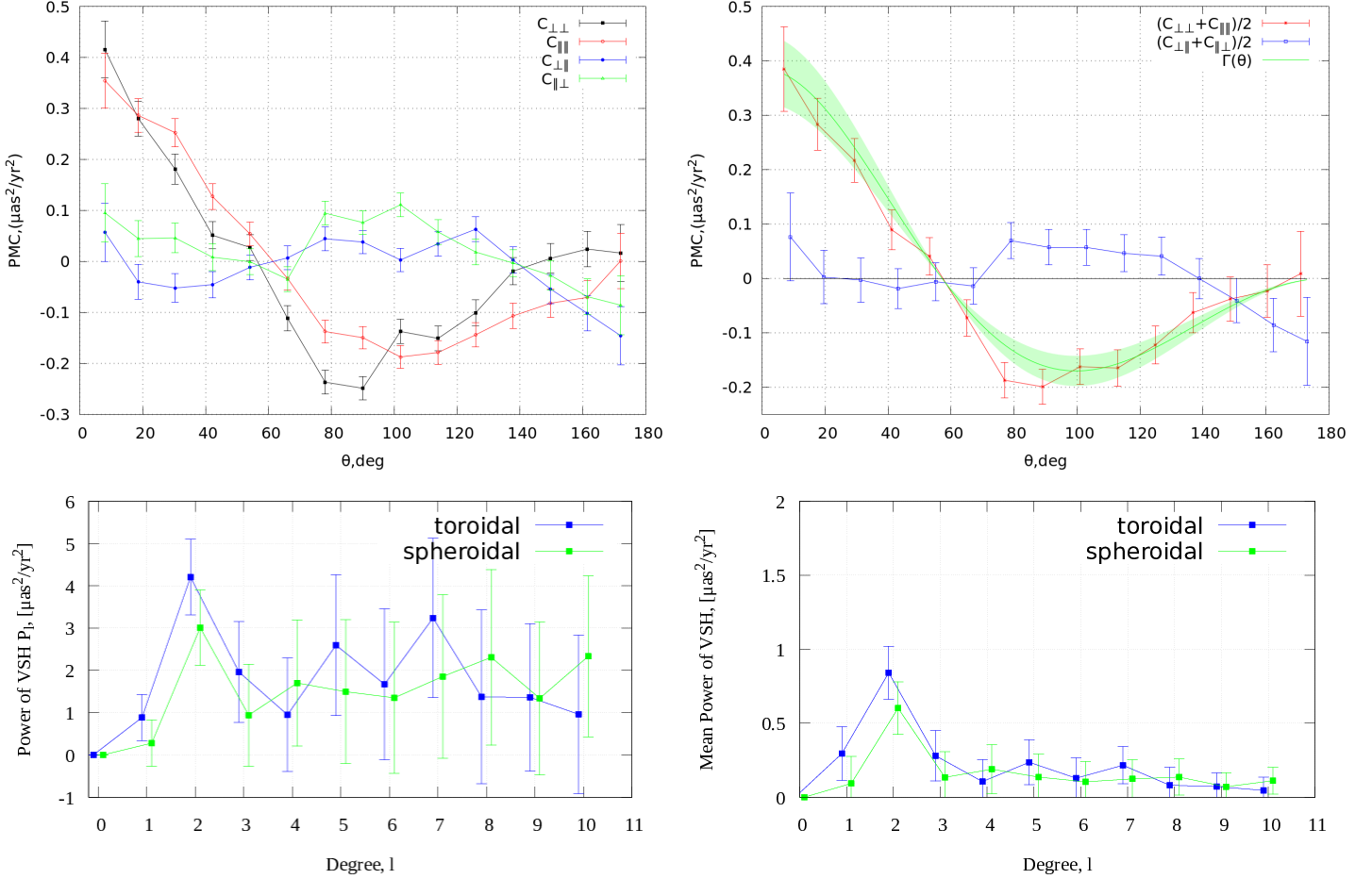


Fig. B.2. Same as Fig. B.1, but applying statistical weights to the quasar proper motions.

Table B.2. Statistical properties of the selected sample of 464 279 quasars, with the noise level reduced by a factor of three relative to the *Gaia*-CRF3 catalogue. The simulated proper motions are less than $100 \mu\text{as yr}^{-1}$.

Name	Mean	SD	Minimum	Maximum	Median	Skewness	Kurtosis
μ_α^* ($\mu\text{as yr}^{-1}$)	-0.00528	44.97	-99.96	99.98	-0.0189	0.00119	-0.738
μ_δ ($\mu\text{as yr}^{-1}$)	0.0972	44.55	-99.96	99.94	0.161	-0.00242	-0.718
$\sigma_{\mu_\alpha^*}$ ($\mu\text{as yr}^{-1}$)	103	74.3	2.92	993	83.9	2.59	11.5
σ_{μ_δ} ($\mu\text{as yr}^{-1}$)	97.3	68.4	3.88	988	79.7	2.70	12.6

model value, corresponding to an underestimation of the GW amplitude by roughly $\sqrt{2}$.

However, the power of higher-order harmonics, particularly $\ell = 5$ and $\ell = 7$, increases by a factor of 2–3. This indicates a pronounced non-uniformity in the sky distribution and in the error properties of the selected sample, leading to the appearance of spurious high-order modes.

These results demonstrate that strong selection cuts on proper motion amplitude introduce significant non-uniformity in the sky distribution of quasars and systematically suppress the low-degree harmonics that encode the GW signal.

The VSH method appears more robust to such selection effects than the HDC approach, as it better isolates the quadrupolar component from higher-order contamination. Nevertheless, severe restrictions of the type $\langle |\mu|/\sigma_\mu \rangle < 2$ can still lead to a systematic underestimation of the GW strain amplitude.

We therefore conclude that proper motion based selection must be applied with caution in GW searches using quasar as-

trometry, as overly strict cuts may bias the inferred GW amplitude.

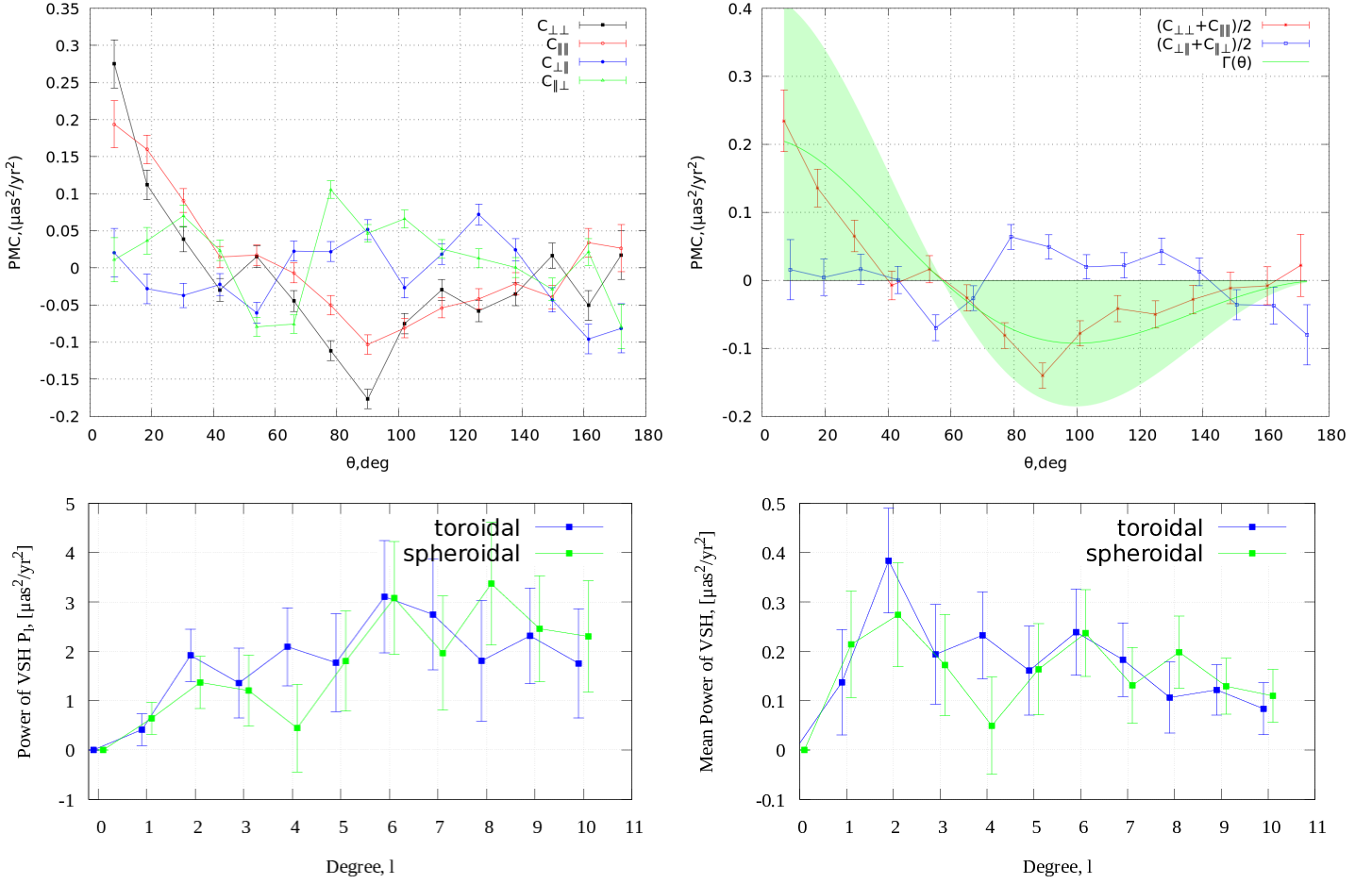


Fig. B.3. Same as Fig.B.1, using statistical weights for the selected 464 279 quasars with simulated proper motion amplitudes less than $100 \mu\text{as yr}^{-1}$.

Table B.3. Statistical properties of the selected sample of 84 607 quasars, with the noise level reduced by a factor of three relative to the *Gaia*-CRF3 catalogue. The simulated proper motions are less than $33 \mu\text{as yr}^{-1}$.

Name	Mean	SD	Minimum	Maximum	Median	Skewness	Kurtosis
μ_α^* ($\mu\text{as yr}^{-1}$)	0.086	15.4	-31.6	31.6	0.083	$1.58\text{e-}4$	-0.937
μ_δ ($\mu\text{as yr}^{-1}$)	0.029	15.4	-31.6	31.6	0.0395	-0.00367	-0.940
$\sigma_{\mu_\alpha^*}$ ($\mu\text{as yr}^{-1}$)	79.2	65.1	2.92	921	60.9	2.94	15.3
σ_{μ_δ} ($\mu\text{as yr}^{-1}$)	75.2	59.8	3.88	973	59.1	3.02	16.3

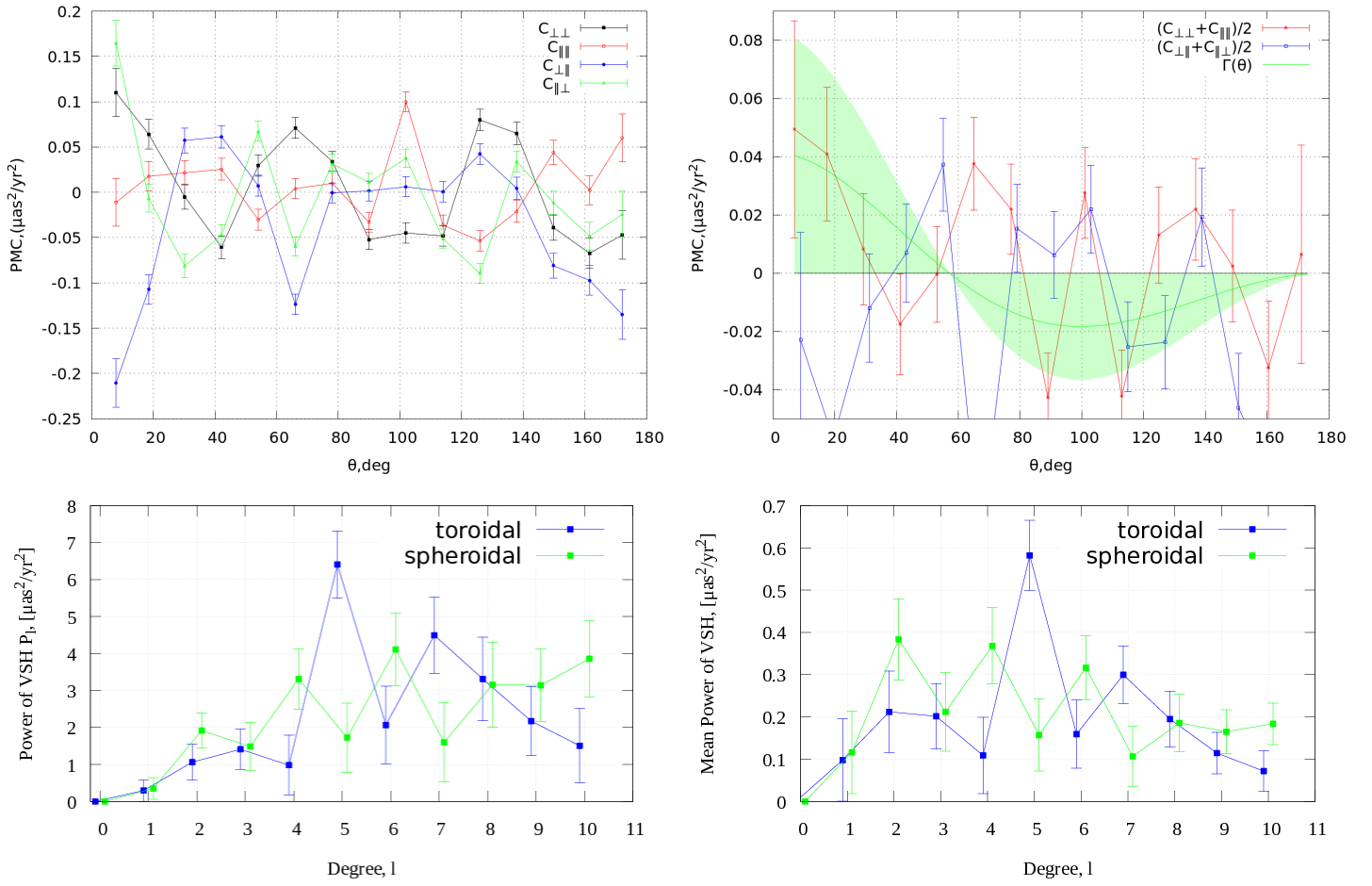


Fig. B.4. Same as Fig. B.1, using statistical weights for the selected 84 607 quasars with simulated proper motion amplitudes less than $33 \mu\text{as yr}^{-1}$.